University of Wollongong

Research Online

Faculty of Engineering and Information Sciences - Papers: Part B

Faculty of Engineering and Information Sciences

2018

Geant4-DNA example applications for track structure simulations in liquid water: A report from the Geant4-DNA Project

Sebastien Incerti
Universite de Bordeaux, incerti@cenbg.in2p3.fr

Ioanna Kyriakou
University of Ioannina Medical School

M A. Bernal
Universidade Estadual de Campinas

M Bordage
Universite Paul Sabatier (Toulouse III)

Z Francis
Universite Saint Joseph

See next page for additional authors

Follow this and additional works at: https://ro.uow.edu.au/eispapers1

 Part of the Engineering Commons, and the Science and Technology Studies Commons

Recommended Citation

Incerti, Sebastien; Kyriakou, Ioanna; Bernal, M A.; Bordage, M; Francis, Z; Guatelli, Susanna; Ivanchenko, Vladimir N.; Karamitros, M; Lampe, N; Lee, Sang Bae; Meylan, Sylvain; Min, C; Shin, W; Nieminen, P; Sakata, Dosatsu; Tang, N; Villagrasa, Carmen; Tran, H; and Brown, J M., "Geant4-DNA example applications for track structure simulations in liquid water: A report from the Geant4-DNA Project" (2018). *Faculty of Engineering and Information Sciences - Papers: Part B*. 1855.
https://ro.uow.edu.au/eispapers1/1855

Research Online is the open access institutional repository for the University of Wollongong. For further information contact the UOW Library: research-pubs@uow.edu.au

Geant4-DNA example applications for track structure simulations in liquid water: A report from the Geant4-DNA Project

Abstract

This Special Report presents a description of Geant4-DNA user applications dedicated to the simulation of track structures (TS) in liquid water and associated physical quantities (e.g., range, stopping power, mean free path.). These example applications are included in the Geant4 Monte Carlo toolkit and are available in open access. Each application is described and comparisons to recent international recommendations are shown (e.g., ICRU, MIRD), when available. The influence of physics models available in Geant4-DNA for the simulation of electron interactions in liquid water is discussed. Thanks to these applications, the authors show that the most recent sets of physics models available in Geant4-DNA (the so-called "option4" and "option 6" sets) enable more accurate simulation of stopping powers, dose point kernels, and W-values in liquid water, than the default set of models ("option 2") initially provided in Geant4-DNA. They also serve as reference applications for Geant4-DNA users interested in TS simulations.

Disciplines

Engineering | Science and Technology Studies

Publication Details

Incerti, S., Kyriakou, I., Bernal, M. A., Bordage, M. C., Francis, Z., Guatelli, S., Ivanchenko, V., Karamitros, M., Lampe, N., Lee, S. B., Meylan, S., Min, C. H., Shin, W. G., Nieminen, P., Sakata, D., Tang, N., Villagrasa, C., Tran, H. N. & Brown, J. M. C. (2018). Geant4-DNA example applications for track structure simulations in liquid water: A report from the Geant4-DNA Project. Medical Physics, 45 (8), e722-e739.

Authors

Sebastien Incerti, Ioanna Kyriakou, M A. Bernal, M Bordage, Z Francis, Susanna Guatelli, Vladimir N. Ivanchenko, M Karamitros, N Lampe, Sang Bae Lee, Sylvain Meylan, C Min, W Shin, P Nieminen, Dosatsu Sakata, N Tang, Carmen Villagrasa, H Tran, and J M. Brown

This journal article is available at Research Online: https://ro.uow.edu.au/eispapers1/1855

Geant4-DNA example applications for track structure simulations in liquid water: a report from the Geant4-DNA Project

S. Incerti[a)]
Univ. Bordeaux, CENBG, UMR 5797, F-33170 Gradignan, France
CNRS, IN2P3, CENBG, UMR 5797, F-33170 Gradignan, France

I. Kyriakou
Medical Physics Laboratory, University of Ioannina Medical School, 45110 Ioannina, Greece

M. A. Bernal
Instituto de Física Gleb Wataghin, Universidade Estadual de Campinas, SP, Brazil

M. C. Bordage
Université Toulouse III-Paul Sabatier, UMR1037 CRCT, Toulouse, France
Inserm, UMR1037 CRCT, Toulouse, France

Z. Francis
Department of Physics, Faculty of Sciences, Université Saint Joseph, Beirut, Lebanon

S. Guatelli
Centre for Medical Radiation Physics, University of Wollongong, Australia
Illawarra Health & Medical Research Institute, University of Wollongong, Australia

V. Ivanchenko

Geant4 Associates International Ltd., Hebden Bridge, United Kingdom

Tomsk State University, Tomsk, Russia

M. Karamitros,

Pessac, France

N. Lampe

Centre Rd, East Bentleigh, Australia

S. B. Lee

Proton Therapy Center, National Cancer Center, 323, Ilsan-ro, Ilsandong-gu, Goyang-si, Gyeonggi-do, Republic of Korea

S. Meylan

SymAlgo Technologies, 75 rue Léon Frot, 75011 Paris, France

C. H. Min, W. G. Shin[b)],

Department of Radiation Convergence Engineering, Yonsei University, Wonju, Republic of Korea

P. Nieminen

ESA-ESTEC, Noordwijk, The Netherlands

D. Sakata

Centre for Medical Radiation Physics, University of Wollongong, Australia

N. Tang, C. Villagrasa
IRSN, Institut de Radioprotection et de Sureté Nucléaire, 92962 Fontenay-aux-Roses, France

H. Tran
IRFU, CEA, Université Paris-Saclay, F-91191 Gif-sur-Yvette, France

J. M. C. Brown
Department of Radiation Science and Technology, Delft University of Technology, Delft, The Netherlands

[a)]Electronic mail: incerti@cenbg.in2p3.fr

[b)]Current address:
Univ. Bordeaux, CENBG, UMR 5797, F-33170 Gradignan, France
CNRS, IN2P3, CENBG, UMR 5797, F-33170 Gradignan, France

Abstract

This Special Report presents a description of Geant4-DNA user applications dedicated to the simulation of track structures (TS) in liquid water and associated physical quantities (e.g. range, stopping power, mean free path...). These example applications are included in the Geant4 Monte Carlo toolkit and are available in open access. Each application is described and comparisons to recent international recommendations are shown (e.g. ICRU, MIRD), when available. The influence of physics models available in Geant4-DNA for the simulation of electron interactions in liquid water is discussed. Thanks to these applications, the authors show that the most recent sets of physics models available in Geant4-DNA (the so-called "option4" and "option 6" sets) enable more accurate simulation of stopping powers, dose point kernels and W-values in liquid water, than the default set of models ("option 2") initially provided in Geant4-DNA. They also serve as reference applications for Geant4-DNA users interested in TS simulations.

Key words: Monte Carlo, track structure, Geant4-DNA, liquid water, dosimetry

I. Introduction

Significant progress has been achieved during the last decades for the development of accurate computational tools capable of simulating mechanistically the passage of radiation through biological matter, especially through the DNA of cell nucleus, which is still considered as the main sensitive site to ionising radiation in cells. This progress is particularly motivated by the need for accurate treatment planning tools for proton/ion-based radiotherapy and for better estimation of the risk to human health during long duration exposure to ionising radiation in manned space missions. Several simulation platforms have been developed so far and are still being extended today by various groups[1], including the state-of-the-art PARTRAC[2] and KURBUC codes[3], which are able to simulate direct and non-direct damage to DNA, including biological repair. Unfortunately, none of them is currently openly accessible to users, preventing from their large-scale usability and adaptability to various user needs.

Alternatively, the Geant4-DNA Project[4-6] (http://geant4-dna.org) proposes the first open access software framework for the simulation of ionising radiation early biological damage at the DNA scale. It is developed by the "Geant4-DNA" Collaboration, which was officially created in 2008. The Geant4-DNA software is an extension to the Geant4 (http://geant4.org) general purpose Monte Carlo toolkit [7-9]. It is entirely included in Geant4 and can be used to simulate step by step physical interactions of particles (electrons, protons, alpha particles including their charged states, and a few ions) down to very low energies (~10 eV) in liquid water and DNA constituents (Adenine, Thymine, Guanine, Cytosine and backbone [10]), thanks to a variety of physics models. It also enables simulation of the physico-chemical and chemical stages of water radiolysis in the irradiated medium up to one microsecond after

irradiation [11], and benefits from the Geant4 ability to model geometries of various biological targets at the micrometer and nanometer scale [12]. We recently demonstrated the combination of the simulation of physical, physico-chemical and chemical interactions with such geometries in order to predict direct and non-direct early DNA damage induction in simplified models of bacterial cells[13-15] and human fibroblasts [16]. Such early damage predictions require an accurate modeling of the track structures of particles in the biological medium[17-19].

Over the last decades, the application of Monte Carlo radiation transport modeling in the field of radiobiology has seen a distinct shift in applicable scale from tissue (millimeter)[20,21] to cellular (micron)[22,23] and, more recently, sub-cellular (nanometer)[24-26] investigations. To ensure the accuracy at these new length scales of interest, it is important to simulate secondary electrons down to the excitation (or ionisation) threshold of the medium, which is in the 7-10 eV range for liquid water. Taking into account the details provided by the simulations, radiation quality and the size of the target to be studied, Monte Carlo codes can be generally classified as condensed history (CH) or track-structure (TS) codes [27]. CH codes group many physical interactions together, speeding up the simulation while reducing the spatial accuracy of local energy deposition. They use multiple scattering theories and stopping power data to be applicable to many materials. Codes such as EGS [28], Geant4 [7-9], PENELOPE [29], MCNP [30], and FLUKA [31], employ the CH technique and are called general purpose Monte Carlo codes because they can be utilized for a variety of applications usually from the keV up to the GeV-TeV energy range, spanning from high energy physics, to medical physics and space radiation applications. Some of these codes, including Geant4, offer a mixed approach which enables separate treatment of “soft” and “hard” collisions, with the latter being simulated in a single-scattering mode. Despite the improved spatial resolution offered by

mixed CH simulations, their application to low-energy (sub-keV) electrons may result in artifacts due to the nature of their physical models which are largely based on high-energy approximations and a combination of different theories [32]. TS codes provide a detailed treatment of all interactions using single-scattering models and thus they offer the appropriate spatial resolution for small biological targets. TS simulations are widely recognized as the preferred approach for micro- and, especially, nano- dosimetry. Several TS codes for radiobiological applications have been developed, with notable examples being the NOREC [33], PARTRAC [34], and KURBUC [35] codes, among others [27]. Recently, the implementation of sophisticated DNA damage and repair pathways in TS codes has been illustrated [36,37]. A few popular general purpose Monte Carlo codes such as PENELOPE[32] and MCNP (version 6[38]) also propose TS simulation capabilities down to low energies (50 eV and 10 eV, respectively).

During the last decade, Geant4-DNA has been equipped with a variety of physics models for the simulation of electron interactions in liquid water enabling Geant4 to perform TS simulations for biological targets. Being fully included in Geant4, these TS simulation capabilities are also accessible via user-friendly wrapper tools like TOPAS[39] and GATE[40] which are based on Geant4. The development of such physics models is an active field of research in theoretical radiation physics [41-43] and it is currently not possible to fully validate these models in the liquid phase of water due to a lack of experimental data [5]. Thus, instead of proposing a single unique model, Geant4-DNA offers a variety of models to simulate the physical interactions of electrons in liquid water and gives the user the freedom of choice. Interactions are grouped in three categories: elastic interactions (that is, elastic scattering), inelastic interactions (electronic excitation and ionisation) and inelastic sub-excitation

interactions (vibrational excitation and molecular attachment, which apply to electrons that do not have sufficient kinetic energy to undergo electronic excitation nor ionisation).

In addition, Geant4-DNA provides users with examples demonstrating how to simulate key quantities regularly studied in the literature, especially for the evaluation of the accuracy of TS codes. Note that Geant4-DNA also proposes other examples[6] for the simulation of water radiolysis and for the modeling of geometries of biological targets - such as DNA -, but their description is beyond the scope of this report, which focuses on (physical) TS simulations in liquid water). In Geant4, an example is a ready-to-use application which is provided with its source code distribution. Today, about 100 such examples are included in Geant4 for a variety of usages. In this work, we present for the first time an overview of the Geant4-DNA examples available to users for TS simulations in liquid water. These examples enable the simulation of a variety of key physical quantities, such as range, stopping power, mean free path, mean energy required for the creation of an ion pair (so-called "W-value"), dose to liquid water target per unit of cumulated activity in a source region ("S-value"), electron slowing down spectra, microdosimetry distributions and dose point kernels. Such examples are used internally on a monthly basis by the Geant4-DNA Collaboration for regression testing of the software and also serve as reference applications for teaching the usage of Geant4-DNA physics models.

II. Geant4-DNA Physics constructors

Geant4-DNA, included in Geant4 version 10.4 (December 2017), currently offers three recommended reference physics constructors for the simulation of discrete particle interactions in liquid water. In Geant4, a physics constructor gathers all required lists of particles, physics processes and associated models required by a Geant4-DNA simulation application. These constructors are referenced as "G4EmDNAPhysics_option2", "G4EmDNAPhysics_option4" and "G4EmDNAPhysics_option6". These three constructors use different physics models for the simulation of electron interactions as will be described later in this section. In this work, they will be referred to as “option 2”, “option 4” and “option 6” constructors, respectively. An overview of the physics processes and models included for the simulation of electron interactions in liquid water is presented in Table 1.

Interactions of protons, neutral hydrogen, alpha particles and their charged states, heavier ions (^{7}Li, ^{9}Be, ^{11}B, ^{12}C, ^{14}N, ^{16}O, ^{28}Si, ^{56}Fe) and photons are handled identically by all three constructors. In brief, nuclear scattering is modelled through classical mechanics[44]. For protons, electronic excitation at low energy (<500 keV) is based on a velocity-scaling of electron excitation cross sections (this approach is also used for hydrogen, and for alpha particles and their charged states) while it uses the Born and Bethe theories at higher energies[5]. Proton ionisation uses a semi-empirical approach at low energy (< 500 keV) while it is based on the Born and Bethe theories and the dielectric formalism for liquid water above this energy[5]. This semi-empirical approach is also used for hydrogen, alpha particles and their charged states, and heavier ions (note that only the ionisation process is currently simulated for these heavier ions). Electron capture and electron loss are described by analytical parametrizations based on experimental data in the vapor phase. The ionisation process for

heavy ions uses a speed scaling of proton ionisation cross section and incorporates the effective charge to take into account the screening of shell electrons[45]. Finally, photon interactions include photoelectric effect, Compton scattering, Rayleigh scattering and pair production, and they are based on the Evaluated Photon Data Library set of models of Geant4[46]. The further detailed description of these models is already available in the literature [5,6,44,45,47-50]. In Table 1 we provide a summary of each Geant4-DNA physics model for electron TS simulations with emphasis on their differences.

II.A. The "Option 2" constructor (default models)

"Option 2" is the first set of discrete physics models implemented in Geant4 for electron transport in liquid water down to eV energies. Since its public release in Geant4 version 9.1 in 2007, it has been the default set of electron models in Geant4-DNA. The inelastic cross sections for the individual ionisation and excitation channels of the weakly-bound electrons of liquid water are calculated numerically from the complex dielectric response function, $\varepsilon(E,q)=\varepsilon_1(E,q)+\varepsilon_2(E,q)$, of the medium with E and q being the energy- and momentum-transfer:

$$\sigma_{n,k}=\int\frac{d\sigma_{n,k}}{dE}\,dE=\frac{1}{\pi a_0 NT}\int dE\int\frac{\mathrm{Im}[\varepsilon_{n,k}(E,q)]}{\left|\varepsilon(E,q)\right|^2}\,\frac{dq}{q} \qquad (1)$$

where σ is the inelastic cross section, a_0 is the Bohr radius, N is the density of water molecules, T is the electron kinetic energy, and the subscripts n, k denote the ionisation shells and excitation levels, respectively. The imaginary part of the dielectric function at the optical limit (q=0), is partitioned to four ionisation shells ($1b_1$, $3a_1$, $1b_2$, $2a_1$) and five discrete

electronic excitations (A^1B_1, B^1A_1, Ryd A+B, Ryd C+D, diffuse bands) according to the parameterization of Emfietzoglou [54]:

$$\mathrm{Im}[\varepsilon(E,q=0)] = \sum_{n=1}^{4}[D_n(E;E_n)\Theta(E-B_n)] + \sum_{k=1}^{5}[D_k^*(E;E_k)\Theta(E-B_k)] \quad (2)$$

where $D_n(E;E_n)$ and $D_k^*(E;E_k)$ are the ordinary and derivative Drude functions with coefficients determined by a fit to optical data under the constraint of the f-sum-rule, and $B_{n,k}$ are threshold energies (e.g. binding energies). The role of the step-functions is to truncate the non-physical contribution of the Drude functions below the threshold values of the corresponding inelastic channels. The real part of the dielectric function is obtained from Eq. (2) using the Kramers-Kronig relation. Extension of the optical dielectric function, $\varepsilon(E,q=0)$, to $q \neq 0$ is made by semi-empirical dispersion relations for the Drude coefficients [55]. Below a few hundred eV, the first Born approximation is not directly applicable; a kinematic Coulomb-field correction and Mott-like exchange-correction terms are used [55]. Total and differential cross sections for electron-impact ionisation of the K-shell (of the oxygen atom) are calculated analytically from the Binary-Encounter-Approximation-with-Exchange model (BEAX) [56]. This is an atomic model which depends only upon the binding energy, mean kinetic energy, and occupation number of the orbital. The scattering angle of the primary electron and the ejection angle of the secondary electron in ionisation events are determined from the kinematics of binary collisions. No angular deflection is considered in collisions leading to electronic excitation. The elastic cross sections are based on partial wave calculations, considering a total interaction potential which takes into account a static contribution as well as fine effects, like exchange and polarization contributions [57]. No energy loss is considered to take place in elastic collisions. Finally, the "option 2" constructor also takes into account the vibrational excitation and electron attachment processes which apply to electrons with kinetic energy lower than the lowest excitation level of liquid water (8.

22 eV). The corresponding models have been derived from experimental data in ice (for vibrational excitation) and vapor phase (for attachment)[58]. These two processes are required for the simulation of electron transport down to thermalization and subsequent water radiolysis[6] (not discussed in this work).

The "option 2" constructor contains the first set of models that were proposed in Geant4-DNA for the modelling of electron interactions in liquid water. However, we recently reported[47] some deficiencies of the default inelastic models due to the truncation of the Drude functions through the step-functions included in Eq. (2). Specifically, Eq. (2) results in the violation of the f-sum-rule, while the expression for $\mathrm{Re}[\varepsilon(E,q)]$ obtained from $\mathrm{Im}[\varepsilon(E,q)]$ via the Kramers-Kronig relation becomes non-trivial. These deficiencies triggered the development of the new "option 4" set of models, as described in the next paragraph.

II.B. The "Option 4" constructor (Ioannina models)

Since Geant4 version 10.2 released in 2016, "option 4" offers alternative discrete physics models to "option 2" (default) for electron transport in liquid water in the 10 eV – 10 keV energy range. "Option 4" (developed at the University of Ioannina) provides updated cross sections for electron impact excitation and ionisation in liquid water, and an alternative elastic scattering model [47,59,60]. Similar to "option 2", inelastic cross sections are calculated from Eq. (1) using the Drude parameterization of $\varepsilon(E,q)$ by Emfietzoglou [54]. Although more advanced dielectric functions are available [42,61], the main advantage of keeping the Drude representation in "option 4" is that due to the mathematical simplicity of the Drude functions both $\mathrm{Im}[\varepsilon(E,q)]$ and $\mathrm{Re}[\varepsilon(E,q)]$ can be expressed analytically and the f-sum-rule is fulfilled for all q regardless of the form of the dispersion relations. The deficiencies related to the

truncation of the Drude functions in "option 2" are overcome in "option 4" through the replacement of Eq. (2) by the following expression [47]:

$$\mathrm{Im}[\varepsilon(E,q=0)] = \sum_{n=1}^{4}\{[D(E;E_n) - D(E;B_n)\exp(B_n - E) + F_n(E)]\Theta(E - B_n)\} + \sum_{k=1}^{5}\{[D_k^*(E;E_k) + F_k(E)]\Theta(E - B_k)\} \quad (3)$$

where $D(E;B_n)\exp(B_n - E)$ is an exponential smoothing function for ionisations, and $F_{n,k}(E)$ are contributions due to the smoothing and truncation of Drude functions at higher energy-levels. The $F_{n,k}(E)$ are calculated analytically by a re-distribution of the oscillator strength in a physically-motivated and f-sum-rule constrained manner [47]. It must be noted that the above modifications have also been used in a recent expression of the dielectric function for liquid water which includes exchange-correlation effects that bring better agreement with the experimental data [62]. Despite starting from essentially the same optical-data model for $\varepsilon(E,q)$ with “option 2”, substantially different ionisation and excitation cross sections are obtained in “option 4”. For example, excitations are strongly enhanced relative to ionisations (which decrease only moderately), resulting in higher mean energies required for the creation of an ion pair in liquid water (the so-called "W-values"), smaller penetration distances, and less diffused dose-point-kernels at sub-keV electron energies[59]. In addition, methodological changes are made in the application of the Coulomb and Mott corrections which result in more accurate ionisation cross sections, especially at energies near the binding energies. These Born corrections account for most of the exchange effects on electron-electron interactions [63,64]. Finally, the elastic cross sections are calculated analytically from the screened Rutherford formula using the screening parameter of Uehara et al. [65] which is deduced from a fit to experimental data for water vapor. The screened Rutherford formula

becomes inaccurate at very low energies and the Brenner-Zaider parametric expression is adopted below 200 eV which fits experimental data in the vapor phase[59]. In the absence of elastic scattering data in liquid water, it is not possible to fully validate such elastic cross sections for the liquid phase. The influence of the water phase at low impact energy is however expected to be small[66].

II.C. The "Option 6" constructor (CPA100 models)

Since Geant4 version 10.4, released in 2017, "option 6" is yet another alternative set of discrete physics models for electron transport in liquid water over the 11 eV - 256 keV energy range. "Option 6" is an implementation of the interaction cross sections of the CPA100 track-structure code to Geant4-DNA[48]. CPA100 was developed and maintained by M. Terrissol et al.[67] and it is one of the few TS codes that can also simulate liquid water radiolysis, such as PARTRAC and KURBUC, among others[27]. The porting of CPA100 to Geant4-DNA enables easy access to these models and further expands their applicability through combination with existing Geant4 functionality (e.g. modelling of complex geometries). Regarding the modeling of track structures, cross sections for electronic excitations are calculated in the first Born approximation using the optical-data model of $\varepsilon(E,q)$ developed by Dingfelder and co-workers [68]. This model is also based on a Drude representation of $\varepsilon(E,q)$, using the same optical data set, electronic excitation levels, and dispersion relations as "option 2" and "option 4". The resulting excitation cross sections, however, are not the same due to a different set of Drude coefficients. The ionisation cross sections for the five shells of water are calculated from the Binary-Encounter-Bethe (BEB) model [69]. Thus, total and differential ionisation cross sections are calculated analytically. Similar to the BEAX model used in "option 2" and "option 4" for electron-impact ionisation of K-shell, the BEB model is an exchange-corrected

atomic model which depends only upon the binding energy, mean kinetic energy, and occupation number of the orbital. Angular deflections in both ionisation and excitation collisions are considered based on the kinematics of binary collisions. Elastic scattering cross sections are based on partial-wave calculations using the independent atom approximation and very small energy loss is taken into account during each single elastic scattering[48].

II.D. Other constructors

All the results presented in this work have been obtained using the "option 2", "option 4" and "option 6" constructors. Other physics constructors have been provided historically with Geant4-DNA. These options are either non-validated (such as “option 1”), obsolete (“option 3”) or accelerated versions of other options for faster computing (e.g., “option 5” is an alternative of “option 4”). "G4EmDNAPhysics" is the default constructor initially delivered to Geant4 in December 2007. This constructor proposes slower versions of the elastic scattering and ionisation processes than the "option 2" constructor, by using non-cumulated differential cross sections for the description of the physical interactions (calculation of scattering angle for elastic scattering and calculation of secondary electron kinetic energy for ionisation); instead "option 2" uses the cumulated version of these differential cross sections. The "G4EmDNAPhysics_option1" constructor uses the "G4LowEWentzelVI" model[70] for the simulation of electron elastic scattering, which is a low-energy extension of the original "WentzelVI" elastic scattering model described in Ref.[71]. Although faster, this model has not been validated compared to existing Geant4-DNA elastic single scattering models and experimental data and is currently provided as a beta development only. The "G4EmDNAPhysics_option3" constructor is obsolete. The "G4EmDNAPhysics_option5" constructor provides an accelerated version of the "option 4" constructor. However, since the

energy applicability of "option 4" is currently limited to 10 keV, this constructor can be used for TS simulations without a strong computing performance penalty while keeping the accuracy of non-cumulated differential cross sections. With the future evolution of the electron ionisation model currently available in "option 4", the usage of "option 5" might become an interesting alternative. Finally, an *ad hoc* constructor is proposed as "G4EmDNAPhysics_option7", combining "option 4" electron models (up to 10 keV) and default Geant4-DNA electron models (from 10 keV up to 1 MeV). This combination is now available through a new software interface ("G4EmDNAPhysicsActivator"), which offers in particular the possibility to track electrons above 1 MeV using Geant4 standard electromagnetic processes and models. This feature will be described later in this work.

III. Geant4-DNA examples for TS simulations in liquid water

Geant4-DNA currently provides 11 examples that can be used to simulate track structures in liquid water. These examples belong to the so-called "extended" category of examples available in the Geant4 toolkit, in parallel to the general "novice" and "advanced" categories of examples which are also available in Geant4. They are all located in the "examples/extended/medical/dna" directory of the toolkit. The list of these examples is summarized in Table 2.

We describe below the main features proposed by these examples, starting from more fundamental examples to a variety of applications. These examples will serve as reference applications for users who have interest in simulating quantities described in Table 2, which are frequently used in TS simulations. We also present and discuss for each example the performance of the three Geant4-DNA physics constructors ("option 2", "option 4" and "option 6") for the simulation of these quantities.

All examples are provided with Geant4 macro files. These macro files are text files which contain Geant4 commands allowing an easy control of the simulation and associated settings, without the need for recompilation of the user application. The names of these macro files are listed in Table 2. Some of the examples also include ROOT [76] macro files for the automatic generation of graphs. These macros contain C++ commands which are directly interpreted by ROOT. The results presented in this work have been obtained exclusively from the described examples, run on a laptop computer equipped with the Geant4 virtual machine (http://geant4.in2p3.fr). These examples can be run in multithreading mode, which allows an

optimized usage of cores and memory in recent computers [9]. The virtual machine contains the full Geant4 installation, ROOT and other tools, and is freely available for download.

III.A. The "dnaphysics" example

- **Purpose**

Historically, the "dnaphysics" example was the first example offered to users illustrating the usage of Geant4-DNA physics processes and models for the simulation of TS in liquid water. This example allows the scoring of all step by step information of particle tracking in liquid water including physical interaction process (e.g. ionisation, electronic excitation...), step position (the so-called pre- and post-step points of each step), local energy deposition, step size, kinetic energy loss, scattering angle and track hierarchy (that is, identification of current step, current track and parent track).

Since release 10.4, this example illustrates the usage of the new "G4EmDNAPhysicsActivator" interface recently added to Geant4. This interface performs the automatic combination of Geant4-DNA models and Geant4 electromagnetic physics models in a geometrical region of the simulated setup specified by the user. This allows for example to simulate the interactions of electrons beyond the 1 MeV maximum upper limit of Geant4-DNA electron models (available in the "option 2" constructor) using Geant4 electromagnetic physics models above this limit. In the current implementation of this interface, Geant4 electromagnetic physics models are taken from the "G4EmStandardPhysics_option4" standard electromagnetic physics constructor of Geant4[9]. Table 3 details the current combination of electron models proposed by this new interface (the

combination for other Geant4-DNA particles, including photons, is described in the Supplemental Table 1).

This new interface can be used in any application directly via User Interface commands and does not require any coding of a combined physics list. Such a combination between Geant4-DNA and Geant4 models, which is not straightforward, was initially demonstrated in the Geant4-DNA "microdosimetry" example [6] where a reference physics list was constructed for users wishing to build their own combination of Geant4-DNA models with Geant4 electromagnetic physics models. This “microdosimetry” example is now kept for preservation.

Alternatively, users can choose to select exclusively any of the Geant4-DNA physics constructors for the tracking of particles. The simulation of atomic relaxation (production of Auger electrons and fluorescence photons [52]) is enabled as well. Atomic relaxation is triggered when ionisation of water K shell occurs. Corresponding transition probabilities and emission energies from oxygen atom are taken from the Evaluated Atomic Data Library (EADL) atomistic database[51] similarly to Geant4 ionising electromagnetic processes, as we recently detailed in Ref.[52,53].

The variable density feature of Geant4 materials is also illustrated by this example: this is an easy way to use the same Geant4-DNA cross sections for a liquid water medium having a density different than the default NIST value used by Geant4-DNA models (i.e. 1 g/cm^3). For example, the state-of-the-art PARTRAC damage simulation software uses a value of 1.06 g/cm^3 for liquid water to approximate cell constituents [78].

- **Results and discussion**

This example can be utilized to study physical processes occurring along particle tracks. As an example, Figure 1 shows the frequency of Geant4-DNA physics processes for 10^2 protons with energy 100 keV, incident in an infinite volume of liquid water. The default Geant4-DNA tracking cut for protons and hydrogen atoms was used (100 eV). The results are presented for the three Geant4-DNA physics constructors, alternatively adopted to describe the particle interactions (note that larger statistics lead to the same observations). The histograms of Figure 1 are automatically generated by the ROOT macro provided with the example. As can be observed from Figure 1, Geant4-DNA physics processes for protons and hydrogen atoms occur with similar frequencies for the three physics constructors. These constructors indeed differ only by the models used to describe electrons interactions, as summarized in Table 1. Figure 1 also illustrates that for the case of the default constructor ("option 2"), vibrational excitation and molecular attachment are activated, while these two processes are not considered by the two other constructors ("option 4" and "option 6"). "Option 2" and "option 6" generate more ionisations than "option 4", which in turn generates more electronic excitations, because of the larger contribution of the excitation cross section, as explained in Ref. [47]. Finally, elastic scattering occurs more frequently in "option 2", since electrons are transported down to 7.4 eV (they are transported down to 10 eV or 11 eV, for “option 4” or “option 6”, respectively - see Table 1).

We provide in Supplemental Figure 1 a visual comparison of three tracks of particles with similar initial velocities simulated using "dnaphysics": a 1 MeV proton, a 4 MeV alpha particle and a 12 MeV carbon ion, over a distance of 500 nm in liquid water, simulated with the "G4EmDNAPhysicsActivator" interface which combines Geant4 electromagnetic physics

models and Geant4-DNA physics models. We used the same color code as in Figure 1 to mark physical interactions. This enabled us to illustrate the "cloud" of electron elastic scattering sites that surrounds the core of the incident particle track and secondary electron tracks.

III.B. The "range" example

- **Purpose**

While the "dnaphysics" example allows for the easy extraction of the main physical quantities of the incident particle and the whole shower of secondary particles created during the tracking, the "range" example simulates the total distance travelled - the so-called "range" - by an incident particle. In this example, the "range" can be tracked until the particle reaches a minimum tracking cut, which can be set by the user, below which this particle is stopped and its remaining kinetic energy is deposited locally into the liquid water medium. In addition, two other quantities are calculated: the "penetration" which represents the distance between the point where the incident particle is shot and the point where its tracking is stopped, and the "projected range" which represents the projection of the "penetration range" along the shooting direction. Naturally, only the incident particle is considered in these simulations. Simulated values are given in nanometers. This example can serve as a benchmark against international recommendations, as we will further discuss below.

- **Results and discussion**

Figure 2 shows the simulation of particle ranges, defined as the sum of all step lengths of the primary particle (electrons, protons, alphas) cumulated over the entire track length, as a function of incident energy, as simulated by the "range" example. For the calculation of electron range, the three Geant4-DNA physics constructors were used with their default tracking cut. For the calculation of proton range, a variable tracking cut has been applied following the procedure initially proposed by Uehara et al. in Ref. [80] and also used in previous Geant4-DNA comparisons [44]. Specifically, the tracking cut has been set to 400 eV at the incident kinetic energy of 1 keV, and to 3 keV at the incident kinetic energy of 500 keV, and its value is interpolated logarithmically for intermediate incident energies. For the simulation of alpha range, the low energy limit of the ionisation model was extended down to 100 eV instead of 1 keV, which is currently the default tracking cut of alpha particles in Geant4-DNA [5]. For comparison, ICRU90 ranges for liquid water are indicated as well [79]. Regarding electrons, below a few keV, "option 2" values are the largest, followed by "option 4" values which are larger than "option 6" values, the latter being closer to ICRU data. Compared to “option 4”, the larger values obtained with “option 2” result mainly from the lower tracking cut proposed by the physics constructor (7.4 eV vs 10 eV). "Option 6" tends to predict systematically shorter ranges especially at the lowest energies. This is a consequence of the larger inelastic cross section for electrons in the 10 eV - 10 keV range available in "option 6" as can be observed in Figure 4 of Ref. [6]. The oscillations observed at very low energy are caused by the rapidly decreasing cross sections for inelastic interactions (including vibrational excitations), as already underlined in Ref. [81] and are not due to statistical fluctuations (10^6 incident electrons were shot for this Figure). Good agreement is observed with the recent ICRU90 recommendations at high energies. Quantitatively, the simulation results start to deviate by more than 10% from ICRU90 recommendations below 10 keV for "option 2" and

"option 4" and below 3 keV for "option 6". Proton ranges agree better than 5% down to 2 keV while alpha ranges deviate by more than 10% below 15 keV.

III.C. The "spower" example

- **Purpose**

Similar to the "range" example, the "spower" example serves as a benchmark to international recommendations on stopping power in liquid water. Simulated values are expressed in MeV/cm for easier comparison to international recommendations. This example activates a stationary mode (frozen-velocity approximation) in models where the incident particle loses energy. In this mode, the kinetic energy of the incident particle is artificially maintained constant at each simulation step. This ensures the correct calculation of the stopping power according to its definition. Secondary particles are not transported during the simulation, and charge exchange processes (electron capture or loss) are considered for protons, hydrogen, alpha particles and their charge states. Nuclear scattering by protons, alpha particles and their charge states can be deactivated if the user is only interested in the simulation of the electronic stopping power.

- **Results and discussion**

Figure 3 shows the simulation of particle stopping power as a function of incident energy, assuming a stationary regime, as explained in the previous section. Electron stopping powers are shown on the left plot, for the three Geant4-DNA physics constructors and on the right plot for protons and alpha particles. Regarding electrons, stopping power calculated using

"option 6" is larger than "option 2" and "option 4" predictions, which is again a consequence of larger inelastic cross sections for "option 6" compared to the two other constructors (similarly, inelastic cross sections are larger for "option 2" than for "option 4", as shown by the corresponding stopping power curves). Regarding comparison to ICRU90 recommendations, Geant4-DNA predictions for electrons are compared to ICRU90 electronic stopping power. "Option 2" and "option 4" values differ from ICRU90 recommendations by 5% and less in the 4 keV - 500 keV range ("option 4" does not go beyond 10 keV), and around 10% down to 1 keV. "Option 6" differs from ICRU90 by less than 4% on the whole energy range covered by this constructor; in particular, it differs by 2% and less below 4 keV down to 1 keV. We should note that ICRU90 stopping power values have a 1.5-5% uncertainty in the range of 1-10 keV. They also neglect shell-corrections which reduce the Bethe stopping power below a few keV[82]. Regarding protons, simulations differ by less than 5% from ICRU90 down to 2 keV. Finally, regarding alpha particles, the differences are larger than 10% below 10 keV and above 150 MeV.

III.D. The "mfp" example

- **Purpose**

The "mfp" example simulates mean-free-path values. This is particularly interesting for the comparison of simulation performance of TS codes for electrons in liquid water at low energies and in small volumes, as for example recently outlined in Emfietzoglou et al. [83]. Users can easily inactivate any Geant4-DNA process thanks to a dedicated process inactivation macro command, allowing, for example, the simulation of inelastic mean-free-

559 path for electrons by having the elastic scattering process switched-off. Simulated mean-free-
560 path values are expressed in nm.
561
562 • **Results and discussion**
563
564 Figure 4 presents electron mean free path as a function of incident energy simulated using the
565 three Geant4-DNA physics constructors. We indicate in these figures mean free paths
566 simulated with all processes active (dashed lines) or with inelastic processes active only (that
567 is ionisation, electronic and vibrational excitation only - solid lines). Globally, for both cases,
568 all curves have similar tendencies. In the case where only inelastic processes are considered,
569 mean free path values obtained with "option 6" are smaller than values simulated with "option
570 4", which follow "option 2" values down to 100 eV. This is a consequence of the dominance
571 of the sum of inelastic cross sections in "option 6" compared to the two other options, as
572 shown in Figure 4 of Ref. [6]. At 100 eV and below, the observed step affecting "option 2"
573 values (solid and dashed red lines) is caused by the vibrational excitation process which
574 becomes active and induces additional energy losses, reducing the mean free path value. In
575 the case where all processes available in physics constructors are active, "option 6" values are
576 systematically smaller than "option 4" values, which tend to become smaller than "option 2"
577 values with decreasing incident energy. As international recommendations (e.g. ICRU
578 reports) for mean free path values are not available yet, it is currently not possible to draw
579 quantitative conclusions on the verification of simulated mean free path values.
580
581 *III.E. The "wvalue" example*
582
583 • **Purpose**

The "wvalue" example is provided in order to evaluate the accuracy of Geant4-DNA constructors for the simulation of the mean energy (the so-called "W-value") required for the creation of an ion pair in liquid water during the slowing-down of an initial particle for given incident energy [47]. This is another benchmark regularly used in the literature to compare TS codes. The user has the possibility to easily select a tracking cut used for the simulation, below which the tracking of particles is stopped and their energy is locally dumped. Simulated W-values are expressed in eV.

- **Results and discussion**

We present in Figure 5 the simulation of W-values for the three Geant4-DNA physics constructors. In these simulations, we have applied the default tracking cut of the constructors (7.4 eV for "option 2", 10 eV for "option 4" and 11 eV for "option 6"). Results are identical to the case where a common tracking cut of 11 eV was used [47], and underline that a small change in the tracking cut does not influence the W-value. For comparison, NOREC [33,86], PARTRAC [33] and RETRACKS [84] simulations and experimental data in gaseous water [85] are shown as well. While "option 2" and "option 6" values remain close down to about 20 eV, "option 4" predictions are the closest to NOREC and PARTRAC simulations; they are also closer to the experimental data set in the gaseous phase, which represents an upper bound of values in the liquid phase [47]. The observed better agreement of "option 4" compared to the two other physics constructors results from the larger ratio of excitation to ionisation cross sections for this constructor.

III.F. The "svalue" example

- **Purpose**

The "svalue" example allows the simulation of S-values which are (mainly) used in targeted radionuclide therapy in order to convert administered activity to radiation dose, as explained by the MIRD committee [73,87]. The S-values represent the dose to a target region per unit of cumulated activity in a source region. The most recent version of the example (which will be released in the near future) simulates the S-values for a spherical shell of liquid water surrounding a plain sphere of liquid water, representing a simplified cytoplasm and nucleus, respectively. Users may select radii and easily change component materials (e.g. liquid water or vacuum). By default, particles are emitted randomly from the cytoplasm volume, a typical configuration for radionuclide therapy in cells [88]. Three configurations can be selected for the description of incident particle emission. Monoenergetic particles are simulated by default. Alternatively, the user can provide a file containing a list of emission energies. The application is adapted to handle such a file in multithreading mode using a dedicated cache mechanism. As a third option, radionuclides, such as Iodine 125 and Iodine 131, can be set as point-like radiation sources. In this case, the radionuclide emission spectrum is directly simulated by the radioactive decay module of Geant4; two macro files are provided as examples. Any radionuclide handled by the radioactive decay module can thus be simulated. Finally, users can also select the tracking cut used in their simulation. The "svalue" example simulates by default S-values for (nucleus ← cytoplasm) and (cytoplasm ← cytoplasm) irradiation, and it can be easily adapted for any other configuration (target ← source). The simulated S-values are expressed in Gy/Bq.s.

- **Results and discussion**

Figure 6 shows the simulation of S-values for a simplified biological cell, containing a spherical nucleus of radius 4 micrometer, surrounded by a spherical cytoplasm of thickness 1 micron. This data was generated by shooting monoenergetic electrons randomly (in position and in direction) from the cytoplasm or from the nucleus. Results are presented for the nucleus as target: either for the (nucleus ← nucleus) configuration (upper curves) or for the (nucleus ← cytoplasm) configuration (lower curves), up to 10 keV, the maximum common high energy limit of physics constructors. Inspection of this figure illustrates a very good agreement between physics constructors. For the configuration where the nucleus is the source, "option 4" differs from "option 2" by less than 1% over the whole energy range and "option 6" differs from "option 2" by less than 1% up to 5 keV and remain below 5% above this energy. Regarding the configuration where the cytoplasm is the source, differences are larger especially for the lowest incident energies: "option 4" differs from "option 2" by less than 5% down to 3 keV and "option 6" differs from "option 2" by less than 10% below 6 keV. This overall agreement between Geant4-DNA constructors has been previously observed when studying the distribution of energy deposition in small spheres of liquid water larger than a few hundreds of nanometers in diameter [60]. S-values for these two configurations have been calculated by the MIRD Committee [89] and are also shown in Figure 6. Regarding the (nucleus ← nucleus) configuration, deviations between the three Geant4-DNA physics constructors and MIRD values are less than 10%, up to about 10 keV. Larger deviations are observed for the (nucleus ← cytoplasm) configuration, especially for the lowest energies, reaching at most 9% at 10 keV and at most 30% at 1 keV both for "option 6". These deviations from MIRD have been already observed, as we presented in Ref. [74]. The public version of this example included in Geant4 10.4 calculates S-values for a single target sphere, whereas the version of this example described in this work will be released in the near future.

III.G. The "slowing" example

- **Purpose**

This example can be used for the simulation of slowing-down spectra of electrons in liquid water. This is another application that is regularly used to compare TS codes [90]. Such spectra represent the fluence distribution (differential in energy) of both the primary and all subsequent generations of secondary electrons generated through the full slowing-down process of the incident particle [72]. The user can activate all atomic de-excitation processes as well as inelastic sub-excitation processes for electrons (vibrational excitation and molecular attachment), as these impact the spectra shape. A tracking cut can also be applied. The simulated slowing-down spectra are expressed as $1/(cm^2.eV.Gy)$.

- **Results and discussion**

Figure 7 presents the simulation of electron slowing-down spectra in liquid water for 100 eV, 1 keV and 10 keV incident monoenergetic electrons, all simulated with the “slowing” example. In these simulations, the elastic scattering process was not considered, except for “option 6” where elastic scatterings are accompanied with small energy losses, as explained in Ref. [48]. Similar results were obtained for “option 2” and “option 4” as we previously described in Ref. [72]: for the 100 eV and 1 keV incident energies, “option 4” values are slightly larger than “option 2” values, down to about 15 eV. This is caused by the lower stopping power values of “option 4” compared to “option 2” (see Figure 3 left panel of this work). “Option 6” values appear systematically lower than the two other constructors. This is

similarly caused by the stopping power values of “option 6” which are larger than the two other constructors (see Figure 3, left panel). The influence of Auger electron production can be observed for all three constructors at the production threshold (around 500 eV) on the 10 keV spectra.

III.H. The "microyz" example

- **Purpose**

The "microyz" example is mainly useful for simulations in microdosimetry [91], a formalism largely used for the investigation of biological effects of ionising radiation at the cellular level (where typical dimensions are of the order of a few microns). It was mainly developed to explain to users how to simulate microdosimetry spectra of lineal energy (usually denoted as "y") and specific energy (usually denoted as "z"), thus the example name "microyz" and their related quantities (frequency-mean and dose-mean averages) in small spheres of liquid water. This example applies a weighting procedure avoiding bias of energy scoring in regions of the full cascade of particles with large number of energy depositions, and is described more fully in other work [60]. Users have the possibility to apply a tracking cut. Lineal energies (in eV/nm) and specific energies (in Gy) are simulated for each incident particle. Corresponding mean values can be calculated using the provided ROOT macro file.

- **Results and discussion**

Performance of the “microyz” extended example has been described in detail in our previous publication (Ref. [60]). As another illustration, we present in Figure 8 the frequency-mean lineal

energy distribution of electrons as a function of their incident kinetic energy, obtained in a 2 nm and 100 nm diameter scoring spheres, for an incident statistics of 10^6 electrons. In order to adopt our previous simulation conditions described in Ref. [60] vibrational excitation and attachment have not been considered for “option 2”. Default tracking cuts have been used for "option 4" (10 eV) and "option 6" (11 eV). A tracking cut of 9 eV (instead of the default value of 7.4 eV) has been used for "option 2", since no energy loss process occurs below 9 eV when vibrational excitation and attachment are not considered (as it is the case in the present simulations).

For the 2 nm sphere, frequency-mean lineal energies obtained with “option 2” and “option 4” constructors are very similar (they differ by less than 10 % over the whole energy range), while “option 6” values are systematically lower by 22% to 36%. This large discrepancy is caused by the numerous very small energy losses occurring during elastic scattering in “option 6” as we explained in [60] and which are accounted for in the calculation of lineal energy values. As an illustration, at 200 eV, when energy losses are not considered during elastic scattering of "option 6", 100% of total energy deposits scored in spheres are larger than 8 eV; on the contrary, when these small energy losses are considered (which is the default setting of "option 6"), about 30% of such deposits are less than 8 eV down to the microeV scale, resulting in a lower frequency-mean lineal energy at this energy, as observed in the left panel of Figure 8. For the 100 nm sphere, although frequency-mean lineal energies have similar trend as a function of incident energy, the values obtained for “option 6” are larger than for “option 4”, the latter being larger than the “option 2” values. Compared to “option 2” values, “option 6” are larger by 7% (at 50 eV) up to 30 % (at 1 keV), and “option 4” values are larger by 7% at 50 eV up to 24 % at 700 eV. The dominance of “option 6” values over the

two other sets results from the larger inelastic cross sections of “option 6”, while these cross sections are in closer agreement for “option 2 “ and “option 4” (see Figure 4 of Ref. [6]).

III.I. The "TestEm12" example

- **Purpose**

This example has not been specifically developed for Geant4-DNA. It is a reference example which can be used with all Geant4 electromagnetic physics models. We recently added the possibility to also use Geant4-DNA physics constructors and a macro file allowing the simulation of dose point kernels (DPK) using these constructors. DPKs serve particularly as benchmarks for the accuracy of electron elastic and inelastic scattering models, as has been previously demonstrated by our Collaboration in Ref. [75]. Energy deposition is recorded in virtual spherical shells around the emission point source and the user can easily select the number of shells using this macro file. Simulated DPK spectra are expressed in MeV/mm as a function of the distance in nm from the point source.

- **Results and discussion**

An extensive verification of DPK distributions has been recently described in Ref. [75], where “option 2”, “option 4” and “option 6” physics constructors have been compared. We show in Figure 9 the DPK obtained for 100 eV and 1 keV incident monoenergetic electrons, using these three constructors with their default tracking cut. We also present DPKs obtained for “option 2” (dashed lines) in the case where inelastic sub-excitation processes (vibrational excitation and attachment) are not considered (these processes are not included in the “option

4" and "option 6" constructors – see Table 1). In all cases, DPKs obtained with "option 2" are more diffusive than the two other constructors (longer tail towards large radius values). At 100 eV, this behavior is clearly magnified when inelastic sub-excitation processes for "option 2" are ignored (dashed red line). This is a direct result of the much lower excitation cross section of "option 2" in comparison to "option 4" and "option 6" [59]. At 1 keV, "option 6" is less diffusive and presents a larger maximum than "option 2" (16% larger and about 4 nm closer to the source) and "option 4" (12% larger and about 4 nm closer to the source). The observed trend (less diffusive DPKs for "option 6" than for the two other constructors) follows the behavior of the total mean free path (which considers elastic and inelastic interactions) as a function of incident energy shown in Figure 4, underlining that models with longer total mean free path lead to more diffusive DPKs. The observed larger maximum of "option 6" is closer to the predictions of the PENELOPE-2011 Monte Carlo code [29] used in a step by step mode in the 1 keV – 10 keV range. The reader is invited to refer to Ref. [75] for more detail regarding the comparison of Geant4-DNA DPKs with the PENELOPE code in this 1 keV – 10 keV energy range.

III.J. The "TestEm5" example

- **Purpose**

"TestEm5" is another Geant4 electromagnetic physics example, which can be used to investigate atomic relaxation. This includes the production of fluorescence photons or Auger electrons after removal of an atomic electron induced by ionisation, the photoelectric effect or Compton scattering processes. This example was used to illustrate the recent addition [52] of Auger cascade simulation in Geant4 electromagnetic physics. Moreover, it has been updated

in order to demonstrate how to mark fluorescence photons and Auger electrons generated from the atomic relaxation cascade induced by the Geant4-DNA ionisation processes. Using a dedicated macro file that fully activates atomic relaxation - including Auger cascades - without any cut for the production of relaxation products, Geant4-DNA users can now easily score the kinetic energy of these particles in histograms.

- **Results and discussion**

Figure 10 (left panel) illustrates the possibility to detect Auger electrons initiated by the Geant4-DNA ionisation process: the number of Auger electrons per incident electron is presented as a function of electron kinetic energy. Auger electrons are generated from the ionised oxygen atom of the water molecule with energies and frequencies tabulated in the EADL database [51]. The three constructors show similar behavior with “option 2” leading to larger production rates compared to “option 4” and “option 6” above 2 keV. For example, at 10 keV, the production of Auger electrons by “option 2” is about 50% larger to “option 4” and “option 6”. On the contrary, at low energy, the production is larger for “option 4” than for the two other constructors. For example, at 1 keV, “option 4” produces about 120% more Auger electrons than “option 2” and about 160% more than “option 6”. The trends of these rates as a function of energy result from the probability of electron-impact ionisation of the K-shell in oxygen atoms, which depends on the modeling of the ionisation process. This probability is represented for a single electron on the right panel of Figure 10 for the three constructors, as a function of the electron energy. It has been calculated as the probability that the incident electron undergoes impact ionisation (among the ionisation, excitation and elastic scattering processes, and using the corresponding cross sections) multiplied by the probability that the ionisation occurs on the K-shell (among the five shells of the water molecule). The

probability obtained with “option 2” is larger than for the two other constructors at high energy, while “option 4” dominates below 1 keV, in agreement with the trends observed in the left panel of Figure 10.

IV. Conclusion

In this work we have reviewed all Geant4-DNA example applications available as part of Geant4 version 10.4 (and some examples soon to be released), for the simulation of track structures in liquid water. This is, to the best knowledge of the authors, the first time that such a variety of examples for TS simulations are made freely available to the community. In addition to their pedagogical role, these examples also serve for evaluating Geant4-DNA physics models' performance and their evolution over time (regression testing). In particular, we have underlined in this work the performance of the recent "option 4" and "option 6" Geant4-DNA physics constructors - developed at Ioannina University (in Greece) and at Paul Sabatier University (in France), respectively - compared to the alternative default constructor "option 2". We have shown that on one hand the "option 6" stopping powers for electrons in liquid water are somewhat closer to the recent ICRU90 recommendations than "option 4" and give larger and less diffusive DPKs, as also predicted by the PENELOPE Monte Carlo code. One should however underline that the less diffusive DPKs predicted by PENELOPE also result from the larger tracking cut of PENELOPE (50 eV versus 7.4 eV for "option 2", 10 eV for "option 4" and 11 eV for "option 6"). On the other hand, "option 4" predicts W-values closer to other Monte Carlo simulations and experimental data in the gas phase than "option 6". In the absence of low energy validation data (< 1 keV) in liquid water, it remains difficult to give a firm recommendation for a specific constructor. However, the usage of these recent constructors could be useful for evaluating quantitatively the dependence of simulation results on such physics models in any user application. In addition to this lack of experimental validation, users should keep in mind that Geant4-DNA (similar to other TS codes) assumes the classical trajectory approximation, which becomes gradually less valid at low energies (especially below 20-50 eV). Such limitations are discussed in detail by Thomson et al. [92] and

838 Liljequist et al. [93] Although it was already shown [47] that “option 4” constructor improves upon
839 “option 2” at various track structure simulations at sub-keV energies, the latter is still used
840 since it covers a larger energy range up to 1 MeV ("option 4" has an upper limit of 10 keV
841 and "option 6" of 256 keV). The “option 4” constructor will soon be extended to relativistic
842 energies, benefiting notably from newly available experimental data and theoretical
843 calculations [83,94], which will extend its usage to a variety of applications beyond 10 keV.
844 These examples will then be used to quantify the impact of such extended models on TS
845 simulations. Regarding the inclusion of cross sections for other materials than liquid water (in
846 particular DNA components or precursors), new cross sections allowing the transport of
847 electrons down to 12 eV and protons used as projectiles (in the range 70 keV-10 MeV)
848 extracted from Ref. [10] have also been included in the Geant4 10.4 release. Their use and
849 validation will be described in a future publication. Moreover, the addition of such other
850 biological materials in the “option 6” constructor as implemented in the CPA100 code, is also
851 planned.
852
853 **Acknowledgements**
854
855 The Geant4-DNA Collaboration acknowledges the following sources of funding and support:
856 the CNRS PICS #7340 France - Greece (2016-2018), the IdEx Bordeaux University - France -
857 International Post-doctorates program in the framework of the "France-Japan Particle Physics
858 Laboratory" International Associated Laboratory (2016-2017) and the IdEx Bordeaux
859 University - France - International Doctorates program in the framework of the "France-
860 Korea Particle Physics Laboratory" International Associated Laboratory (2017-2020). M. A.
861 Bernal acknowledges the support received from the Conselho Nacional para o
862 Desenvolvimento Científico e Tecnológico (CNPq), Brazil, for financing his research

activities through the project 306775/2015-8. S. Guatelli and D. Sakata acknowledge the financial support of the Australian Research Council, ARC DP170100967. I. Kyriakou acknowledges financial support from ESA (Contract No. 4000112863/14/NL/HB).

The authors have no conflicts to disclose.

References

[1] I. El Naqa, P. Pater, and J. Seuntjens, Physics in Medicine and Biology **57,** R75 (2012).

[2] W. Friedland, E. Schmitt, P. Kundrát, M. Dingfelder, G. Baiocco, S. Barbieri, and A. Ottolenghi, Scientific Reports **7,** 45161 (2017).

[3] H. Nikjoo, D. Emfietzoglou, T. Liamsuwan, R. Taleei, D. Liljequist, and S. Uehara, Reports on Progress in Physics **79,** 116601 (2016).

[4] S. Incerti, G. Baldacchino, M. Bernal, R. Capra, C. Champion, Z. Francis, P. Guèye, A. Mantero, B. Mascialino, P. Moretto, P. Nieminen, C. Villagrasa, and C. Zacharatou, International Journal of Modeling, Simulation, and Scientific Computing **01,** 157 (2010).

[5] S. Incerti, A. Ivanchenko, M. Karamitros, A. Mantero, P. Moretto, H. N. Tran, B. Mascialino, C. Champion, V. N. Ivanchenko, M. A. Bernal, Z. Francis, C. Villagrasa, G. Baldacchino, P. Guèye, R. Capra, P. Nieminen, and C. Zacharatou, Medical Physics **37,** 4692 (2010).

[6] M. A. Bernal, M. C. Bordage, J. M. C. Brown, M. Davídková, E. Delage, Z. El Bitar, S. A. Enger, Z. Francis, S. Guatelli, V. N. Ivanchenko, M. Karamitros, I. Kyriakou, L. Maigne, S. Meylan, K. Murakami, S. Okada, H. Payno, Y. Perrot, I. Petrovic, Q. T. Pham, A. Ristic-Fira, T. Sasaki, V. Štěpán, H. N. Tran, C. Villagrasa, and S. Incerti, Physica Medica **31,** 861 (2015).

[7] S. Agostinelli, J. Allison, K. Amako, J. Apostolakis, H. Araujo, P. Arce, M. Asai, D. Axen, S. Banerjee, G. Barrand, F. Behner, L. Bellagamba, J. Boudreau, L. Broglia, A. Brunengo, H. Burkhardt, S. Chauvie, J. Chuma, R. Chytracek, G. Cooperman, G. Cosmo, P. Degtyarenko, A. Dell'Acqua, G. Depaola, D. Dietrich, R. Enami, A. Feliciello, C. Ferguson, H. Fesefeldt, G. Folger, F. Foppiano, A. Forti, S. Garelli, S. Giani, R. Giannitrapani, D. Gibin, J. J. Gómez Cadenas, I. González, G. Gracia Abril, G. Greeniaus, W. Greiner, V. Grichine, A. Grossheim, S. Guatelli, P. Gumplinger, R. Hamatsu, K. Hashimoto, H. Hasui, A. Heikkinen, A. Howard, V. Ivanchenko, A. Johnson, F. W. Jones, J. Kallenbach, N. Kanaya, M. Kawabata, Y. Kawabata, M. Kawaguti, S. Kelner, P. Kent, A. Kimura, T. Kodama, R. Kokoulin, M. Kossov, H. Kurashige, E. Lamanna, T. Lampén, V. Lara, V. Lefebure, F. Lei, M. Liendl, W. Lockman, F. Longo, S. Magni, M. Maire, E. Medernach, K. Minamimoto, P. Mora de Freitas, Y. Morita, K. Murakami, M. Nagamatu, R. Nartallo, P. Nieminen, T. Nishimura, K. Ohtsubo, M. Okamura, S. O'Neale, Y. Oohata, K. Paech, J. Perl, A. Pfeiffer, M. G. Pia, F. Ranjard, A. Rybin, S. Sadilov, E. Di Salvo, G. Santin, T. Sasaki, N. Savvas, Y. Sawada, Nuclear Instruments and Methods in Physics Research Section A: Accelerators, Spectrometers, Detectors and Associated Equipment **506,** 250 (2003).

[8] J. Allison, K. Amako, J. Apostolakis, H. Araujo, P. A. Dubois, M. Asai, G. Barrand, R. Capra, S. Chauvie, R. Chytracek, G. A. P. Cirrone, G. Cooperman, G. Cosmo, G. Cuttone, G. G. Daquino, M. Donszelmann, M. Dressel, G. Folger, F. Foppiano, J. Generowicz, V. Grichine, S. Guatelli, P. Gumplinger, A. Heikkinen, I. Hrivnacova, A. Howard, S. Incerti, V. Ivanchenko, T. Johnson, F. Jones, T. Koi, R. Kokoulin, M. Kossov, H. Kurashige, V. Lara, S. Larsson, F. Lei, O. Link, F. Longo, M. Maire, A. Mantero, B. Mascialino, I. McLaren, P. M. Lorenzo, K. Minamimoto, K. Murakami, P. Nieminen, L. Pandola, S. Parlati, L. Peralta, J. Perl, A. Pfeiffer, M. G. Pia, A. Ribon,

P. Rodrigues, G. Russo, S. Sadilov, G. Santin, T. Sasaki, D. Smith, N. Starkov, S. Tanaka, E. Tcherniaev, B. Tome, A. Trindade, P. Truscott, L. Urban, M. Verderi, A. Walkden, J. P. Wellisch, D. C. Williams, D. Wright, and H. Yoshida, Nuclear Science, IEEE Transactions on **53,** 270 (2006).

9 J. Allison, K. Amako, J. Apostolakis, P. Arce, M. Asai, T. Aso, E. Bagli, A. Bagulya, S. Banerjee, G. Barrand, B. R. Beck, A. G. Bogdanov, D. Brandt, J. M. C. Brown, H. Burkhardt, P. Canal, D. Cano-Ott, S. Chauvie, K. Cho, G. A. P. Cirrone, G. Cooperman, M. A. Cortés-Giraldo, G. Cosmo, G. Cuttone, G. Depaola, L. Desorgher, X. Dong, A. Dotti, V. D. Elvira, G. Folger, Z. Francis, A. Galoyan, L. Garnier, M. Gayer, K. L. Genser, V. M. Grichine, S. Guatelli, P. Guèye, P. Gumplinger, A. S. Howard, I. Hřivnáčová, S. Hwang, S. Incerti, A. Ivanchenko, V. N. Ivanchenko, F. W. Jones, S. Y. Jun, P. Kaitaniemi, N. Karakatsanis, M. Karamitros, M. Kelsey, A. Kimura, T. Koi, H. Kurashige, A. Lechner, S. B. Lee, F. Longo, M. Maire, D. Mancusi, A. Mantero, E. Mendoza, B. Morgan, K. Murakami, T. Nikitina, L. Pandola, P. Paprocki, J. Perl, I. Petrović, M. G. Pia, W. Pokorski, J. M. Quesada, M. Raine, M. A. Reis, A. Ribon, A. Ristić Fira, F. Romano, G. Russo, G. Santin, T. Sasaki, D. Sawkey, J. I. Shin, I. I. Strakovsky, A. Taborda, S. Tanaka, B. Tomé, T. Toshito, H. N. Tran, P. R. Truscott, L. Urban, V. Uzhinsky, J. M. Verbeke, M. Verderi, B. L. Wendt, H. Wenzel, D. H. Wright, D. M. Wright, T. Yamashita, J. Yarba, and H. Yoshida, Nuclear Instruments and Methods in Physics Research Section A: Accelerators, Spectrometers, Detectors and Associated Equipment **835,** 186 (2016).

10 M. U. Bug, W. Yong Baek, H. Rabus, C. Villagrasa, S. Meylan, and A. B. Rosenfeld, Radiation Physics and Chemistry **130,** 459 (2017).

11 M. Karamitros, S. Luan, M. A. Bernal, J. Allison, G. Baldacchino, M. Davidkova, Z. Francis, W. Friedland, V. Ivantchenko, A. Ivantchenko, A. Mantero, P. Nieminem, G. Santin, H. N. Tran, V. Stepan, and S. Incerti, Journal of Computational Physics **274,** 841 (2014).

12 S. Incerti, M. Douglass, S. Penfold, S. Guatelli, and E. Bezak, Physica Medica: European Journal of Medical Physics **32,** 1187 (2016).

13 N. Lampe, Thesis, Université Clermont Auvergne, 2017.

14 N. Lampe, M. Karamitros, V. Breton, J. M. C. Brown, I. Kyriakou, D. Sakata, D. Sarramia, and S. Incerti, Physica Medica: European Journal of Medical Physics **48,** 135 (2018).

15 N. Lampe, M. Karamitros, V. Breton, J. M. C. Brown, D. Sakata, D. Sarramia, and S. Incerti, Physica Medica: European Journal of Medical Physics **48,** 146 (2018).

16 S. Meylan, S. Incerti, M. Karamitros, N. Tang, M. Bueno, I. Clairand, and C. Villagrasa, Scientific Reports **7,** 11923 (2017).

17 H. Nikjoo, R. Taleei, T. Liamsuwan, D. Liljequist, and D. Emfietzoglou, Radiation Physics and Chemistry **128,** 3 (2016).

18 M. Dingfelder, I. G. Jorjishvili, J. A. Gersh, and L. H. Toburen, Radiation Protection Dosimetry **122,** 26 (2006).

19 H. Nikjoo, D. Emfietzoglou, R. Watanabe, and S. Uehara, Radiation Physics and Chemistry **77,** 1270 (2008).

20 C. L. H. Siantar, R. S. Walling, T. P. Daly, B. Faddegon, N. Albright, P. Bergstrom, A. F. Bielajew, C. Chuang, D. Garrett, R. K. House, D. Knapp, D. J. Wieczorek, and L. J. Verhey, Medical Physics **28,** 1322 (2001).

21 L. Strigari, E. Menghi, M. D'Andrea, and M. Benassi, Medical Physics **33,** 3383 (2006).

964 [22] J. Lehmann, C. Siantar Hartmann, D. E. Wessol, C. A. Wemple, D. Nigg, J. Cogliati, T.
965 Daly, M.-A. Descalle, T. Flickinger, D. Pletcher, and G. DeNardo, Physics in
966 Medicine & Biology **50,** 947 (2005).
967 [23] N. Falzone, J. M. Fernández-Varea, G. Flux, and K. A. Vallis, Journal of Nuclear
968 Medicine **56,** 1441 (2015).
969 [24] C. Bousis, D. Emfietzoglou, and H. Nikjoo, Int J Radiat Biol **88,** 908 (2012).
970 [25] D. J. Carlson, R. D. Stewart, V. A. Semenenko, and G. A. Sandison, Radiation
971 Research **169,** 447 (2008).
972 [26] V. A. Semenenko, R. D. Stewart, and E. J. Ackerman, Radiation Research **164,** 180
973 (2005).
974 [27] H. Nikjoo, S. Uehara, D. Emfietzoglou, and F. Cucinotta, Radiation Measurements
975 **41,** 1052 (2006).
976 [28] I. Kawrakow, E. Mainegra-Hing, D. W. O. Rogers, F. Tessier, and B. R. B. Walters,
977 NRCC Report PIRS-701 (2017).
978 [29] J. Baró, J. Sempau, J. M. Fernández-Varea, and F. Salvat, Nuclear Instruments and
979 Methods in Physics Research Section B: Beam Interactions with Materials and
980 Atoms **100,** 31 (1995).
981 [30] J. F. Briesmeister, *MCNP-A general Monte Carlo code for neutron and photon*
982 *transport*, Vol. LA-7396-M 3A (Los Alamos National Laboratory, Los Alamos,
983 1986).
984 [31] A. Ferrari, P. R. Sala, A. Fasso, and J. Ranft, *FLUKA: A multi-particle transport code*
985 *(Program version 2005)* (CERN, Geneva, 2005).
986 [32] J. M. Fernández-Varea, G. González-Muñoz, M. E. Galassi, K. Wiklund, B. K. Lind, A.
987 Ahnesjö, and N. Tilly, International Journal of Radiation Biology **88,** 66 (2012).
988 [33] M. Dingfelder, R. H. Ritchie, J. E. Turner, W. Friedland, H. G. Paretzke, and R. N.
989 Hamm, Radiation Research **169,** 584 (2008).
990 [34] W. Friedland, M. Dingfelder, P. Kundrát, and P. Jacob, Mutation
991 Research/Fundamental and Molecular Mechanisms of Mutagenesis **711,** 28
992 (2011).
993 [35] T. Liamsuwan, D. Emfietzoglou, S. Uehara, and H. Nikjoo, International Journal of
994 Radiation Biology **88,** 899 (2012).
995 [36] R. Taleei and H. Nikjoo, International Journal of Radiation Biology **88,** 948
996 (2012).
997 [37] R. Taleei, P. M. Girard, K. Sankaranarayanan, and H. Nikjoo, Radiation Research
998 **179,** 540 (2013).
999 [38] J. T. Goorley, M. R. James, T. E. Booth, F. B. Brown, J. S. Bull, L. J. Cox, J. W. Durkee,
1000 Jr., J. S. Elson, M. L. Fensin, R. A. Forster, III, J. S. Hendricks, H. G. Hughes, III, R. C.
1001 Johns, B. C. Kiedrowski, R. L. Martz, S. G. Mashnik, G. W. McKinney, D. B. Pelowitz,
1002 R. E. Prael, J. E. Sweezy, L. S. Waters, T. Wilcox, and A. J. Zukaitis, "Initial MCNP6
1003 Release Overview - MCNP6 version 1.0," (2013).
1004 [39] A. L. McNamara, C. Geng, R. Turner, M. J. R., J. Perl, K. Held, B. Faddegon, H.
1005 Paganetti, and J. Schuemann, Phys. Med. **33,** 207 (2017).
1006 [40] Q. T. Pham, A. Anne, M. Bony, E. Delage, D. Donnarieix, A. Dufaure, M. Gautier, S. B.
1007 Lee, P. Micheau, G. Montarou, Y. Perrot, J. I. Shin, S. Incerti, and L. Maigne, Nuclear
1008 Instruments and Methods in Physics Research Section B: Beam Interactions with
1009 Materials and Atoms **353,** 46 (2015).
1010 [41] M. Dingfelder, Applied Radiation and Isotopes **83, Part B,** 142 (2014).
1011 [42] D. Emfietzoglou, I. Kyriakou, I. Abril, R. Garcia-Molina, and H. Nikjoo,
1012 International Journal of Radiation Biology **88,** 22 (2012).

[43] J. Fernandez-Varea, F. Salvat, M. Dingfelder, and D. Liljequist, Nuclear Instruments and Methods in Physics Research Section B: Beam Interactions with Materials and Atoms **229,** 187 (2005).
[44] H. N. Tran, Z. El Bitar, C. Champion, M. Karamitros, M. A. Bernal, Z. Francis, V. Ivantchenko, S. B. Lee, J. I. Shin, and S. Incerti, Nuclear Instruments and Methods in Physics Research Section B: Beam Interactions with Materials and Atoms **343,** 132 (2015).
[45] Z. Francis, S. Incerti, V. Ivanchenko, C. Champion, M. Karamitros, M. A. Bernal, and Z. E. Bitar, Physics in Medicine and Biology **57,** 209 (2012).
[46] D. E. Cullen, J. H. Hubbell, and L. Kissel, *EPDL97: The evaluated photon data library, 97 version*, Vol. UCRL-LR-50400-V6-R5 (Lawrence Livermore National Laboratory, Livermore, 1997).
[47] I. Kyriakou, S. Incerti, and Z. Francis, Medical Physics **42,** 3870 (2015).
[48] M. C. Bordage, J. Bordes, S. Edel, M. Terrissol, X. Franceries, M. Bardiès, N. Lampe, and S. Incerti, Physica Medica: European Journal of Medical Physics **32,** 1833 (2016).
[49] M. Michaud, A. Wen, and L. Sanche, Radiation Research **159,** 3 (2003).
[50] C. E. Melton, The Journal of Chemical Physics **57,** 4218 (1972).
[51] S. T. Perkins, D. Cullen, M. Chen, J. Rathkopf, J. Scofield, and J. Hubbell, *Tables and graphs of atomic subshell and relaxation data derived from the LLNL Evaluated Atomic Data Library (EADL), Z= 1-100*, Vol. UCRL-50400-V30 (Lawrence Livermore National Laboratory, Livermore, 1991).
[52] S. Incerti, B. Suerfu, J. Xu, V. Ivantchenko, A. Mantero, J. M. C. Brown, M. A. Bernal, Z. Francis, M. Karamitros, and H. N. Tran, Nuclear Instruments and Methods in Physics Research Section B: Beam Interactions with Materials and Atoms **372,** 91 (2016).
[53] A. Mantero, H. Ben Abdelouahed, C. Champion, Z. El Bitar, Z. Francis, P. Guèye, S. Incerti, V. Ivanchenko, and M. Maire, X-Ray Spectrometry **40,** 135 (2011).
[54] D. Emfietzoglou, Radiation Physics and Chemistry **66,** 373 (2003).
[55] D. Emfietzoglou and H. Nikjoo, Radiation Research **163,** 98 (2005).
[56] M. Rudd, Y.-K. Kim, T. Märk, J. Schou, N. Stolterfoht, and L. Toburen, (1996).
[57] C. Champion, S. Incerti, H. Aouchiche, and D. Oubaziz, Radiation Physics and Chemistry **78,** 745 (2009).
[58] Z. Francis, S. Incerti, R. Capra, B. Mascialino, G. Montarou, V. Stepan, and C. Villagrasa, Applied Radiation and Isotopes **69,** 220 (2011).
[59] I. Kyriakou, M. Šefl, V. Nourry, and S. Incerti, Journal of Applied Physics **119,** 194902 (2016).
[60] I. Kyriakou, D. Emfietzoglou, V. Ivanchenko, M. C. Bordage, S. Guatelli, P. Lazarakis, H. N. Tran, and S. Incerti, Journal of Applied Physics **122,** 024303 (2017).
[61] D. Emfietzoglou, I. Kyriakou, R. Garcia-Molina, and I. Abril, Surface and Interface Analysis **49,** 4 (2017).
[62] D. Emfietzoglou, F. A. Cucinotta, and H. Nikjoo, Radiation Research **164,** 202 (2005).
[63] D. Emfietzoglou, I. Kyriakou, R. Garcia-Molina, I. Abril, and H. Nikjoo, Radiation Research **180,** 499 (2013).
[64] D. Emfietzoglou, I. Kyriakou, R. Garcia-Molina, and I. Abril, Journal of Applied Physics **114,** 144907 (2013).

[65] S. Uehara, H. Nikjoo, and D. T. Goodhead, Physics in Medicine and Biology **38,** 1841 (1993).
[66] H. Aouchiche, C. Champion, and D. Oubaziz, Radiation Physics and Chemistry **77,** 107 (2008).
[67] M. Terrissol and A. Beaudré, Radiation Protection Dosimetry **31,** 175 (1990).
[68] M. Dingfelder, D. Hantke, M. Inokuti, and H. G. Paretzke, Radiation Physics and Chemistry **53,** 1 (1999).
[69] Y.-K. Kim and M. E. Rudd, Physical Review A **50,** 3954 (1994).
[70] J. Apostolakis, M. Asai, A. Bagulya, J. M. C. Brown, H. Burkhardt, N. Chikuma, M. A. Cortes-Giraldo, S. Elles, V. Grichine, S. Guatelli, S. Incerti, V. N. Ivanchenko, J. Jacquemier, O. Kadri, M. Maire, L. Pandola, D. Sawkey, T. Toshito, L. Urban, and T. Yamashita, Journal of Physics: Conference Series **664,** 072021 (2015).
[71] V. N. Ivanchenko, O. Kadri, M. Maire, and L. Urban, Journal of Physics: Conference Series **219,** 032045 (2010).
[72] S. Incerti, I. Kyriakou, and H. N. Tran, Nuclear Instruments and Methods in Physics Research Section B: Beam Interactions with Materials and Atoms **397,** 45 (2017).
[73] T. André, F. Morini, M. Karamitros, R. Delorme, C. Le Loirec, L. Campos, C. Champion, J. E. Groetz, M. Fromm, M. C. Bordage, Y. Perrot, P. Barberet, M. A. Bernal, J. M. C. Brown, M. S. Deleuze, Z. Francis, V. Ivanchenko, B. Mascialino, C. Zacharatou, M. Bardiès, and S. Incerti, Nuclear Instruments and Methods in Physics Research Section B: Beam Interactions with Materials and Atoms **319,** 87 (2014).
[74] M. Šefl, S. Incerti, G. Papamichael, and D. Emfietzoglou, Applied Radiation and Isotopes **104,** 113 (2015).
[75] J. Bordes, S. Incerti, N. Lampe, M. Bardiès, and M.-C. Bordage, Nuclear Instruments and Methods in Physics Research Section B: Beam Interactions with Materials and Atoms **398,** 13 (2017).
[76] R. Brun and F. Rademakers, Nuclear Instruments and Methods in Physics Research Section A: Accelerators, Spectrometers, Detectors and Associated Equipment **389,** 81 (1997).
[77] J. M. C. Brown, M. R. Dimmock, J. E. Gillam, and D. M. Paganin, Nuclear Instruments and Methods in Physics Research Section B: Beam Interactions with Materials and Atoms **338,** 77 (2014).
[78] W. Friedland, P. Jacob, P. Bernhardt, H. G. Paretzke, and M. Dingfelder, Radiation Research **159,** 401 (2003).
[79] S. Seltzer, J. Fernández-Varea, P. Andreo, P. Bergstrom, D. Burns, I. Krajcar Bronić, C. Ross, and F. Salvat, (2016).
[80] S. Uehara, L. Toburen, and H. Nikjoo, International journal of radiation biology **77,** 139 (2001).
[81] Z. Francis, S. Incerti, M. Karamitros, H. N. Tran, and C. Villagrasa, Nuclear Instruments and Methods in Physics Research Section B: Beam Interactions with Materials and Atoms **269,** 2307 (2011).
[82] D. Emfietzoglou and H. Nikjoo, Radiation Research **167,** 110 (2007).
[83] D. Emfietzoglou, G. Papamichael, and H. Nikjoo, Radiation Research **188,** 355 (2017).
[84] I. Plante and F. A. Cucinotta, New Journal of Physics **11,** 063047 (2009).
[85] D. Combecher, Radiation Research **84,** 189 (1980).

86 V. A. Semenenko, J. E. Turner, and T. B. Borak, Radiation and Environmental Biophysics **42,** 213 (2003).

87 S. M. Goddu, *MIRD Cellular S values: Self-absorbed dose per unit cumulated activity for selected radionuclides and monoenergetic electron and alpha particle emitters incorporated into different cell compartments* (Society of Nuclear Medicine, 1997).

88 H. Uusijärvi, P. Bernhardt, T. Ericsson, and E. Forssell-Aronsson, Medical Physics **33,** 3260 (2006).

89 S. M. Goddu, R. Howell, L. Bouchet, W. Bolch, and D. V. Rao, Reston, VA: Society of Nuclear Medicine (1997).

90 O. N. Vassiliev, Physics in Medicine & Biology **57,** 1087 (2012).

91 H. H. Rossi and M. Zaider, *Microdosimetry and its Applications* (Springer, 1996).

92 R. M. Thomson and I. Kawrakow, Medical Physics **38,** 4531 (2011).

93 D. Liljequist and H. Nikjoo, Radiation Physics and Chemistry **99,** 45 (2014).

94 H. Hayashi and N. Hiraoka, The Journal of Physical Chemistry B **119,** 5609 (2015).

Figure 1: Illustration of the usage of the "dnaphysics" example for the scoring of Geant4-DNA processes occurring along 10^2 incident proton tracks of 100 keV in an infinite volume of liquid water. The left plot has been obtained with Geant4-DNA physics constructor "option 2" (default models), the middle plot with "option 4" (Ioannina U. models) and the right one with "option 6" (CPA100 models). Occurrences are represented by vertical bars, as a function of particle type. The numbers indicated on the horizontal axis are used to identify processes in the application.

Figure 2: Electron, proton and alpha ranges (all represented as solid lines) in liquid water simulated using the "range" example as a function of incident kinetic energy. For electrons, results obtained for the three Geant4-DNA physics constructors are indicated (in red for "option 2", in green for "option 4" and in blue for "option 6"). Symbols represent the recent ICRU90 recommendations [79].

Figure 3: Stopping power for electrons (left plot, solid lines), protons and alpha particles (right plot, solid lines) in liquid water as a function of incident energy, simulated with the "spower" example. For electrons, results obtained for the three Geant4-DNA physics constructors are indicated (in red for "option 2", in green for "option 4" and in blue for "option 6"). Symbols represent the recent corresponding ICRU90 recommendations for stopping power (electronic stopping power on left plot, total stopping power on right plot) [79].

Figure 4: Mean free path for electrons in liquid water, considering all physical interactions (dashed lines) or inelastic interactions only (solid lines) as a function of incident particle energy, simulated with the "mfp" example, for the three Geant4-DNA physics constructors.

Figure 5: W-value for electrons as a function of incident energy up to 100 keV in liquid water simulated using the "wvalue" example, for the three Geant4-DNA constructors. Monte Carlo simulations from NOREC (dashed line, Ref. [33]), PARTRAC (dotted line, Ref. [33]), RETRACKS (dash-dotted line, Ref. [84]) and experimental data in gaseous water (squares, Ref. [85]) are shown as well for comparison.

Figure 6: S-values for the nucleus ← nucleus (denoted as "N ← N") and the nucleus ← cytoplasm (denoted as "N ← Cy") configurations, in a simplified spherical cell (nucleus of radius 4 microns and cytoplasm of thickness 1 micron - as shown in the inset), as a function of incident electron energy in liquid water simulated using the "svalue" example, for the three Geant4-DNA constructors (colored circles). MIRD calculations are indicated as well (black stars) [89].

Figure 7: Slowing-down spectra in liquid water for 100 eV, 1 keV and 10 keV monoenergetic electrons simulated with the "slowing" example using the three Geant4-DNA physics constructors.

Figure 8: Frequency-mean lineal energy (y_F) as a function of incident electron kinetic energy for a scoring sphere of diameter 2 nm (left panel) and 100 nm (right panel). These distributions have been simulated with the "microyz" example for the three Geant4-DNA physics constructors.

Figure 9: Dose point kernels (DPK) for 10^6 monoenergetic electrons of 100 eV and 1 keV in liquid water, simulated using the "TestEm12" extended example. Results are shown for the three Geant4-DNA physics constructors. The red dashed lines show "option 2" DPKs when

inelastic sub-excitation processes (vibrational excitation and attachment) are not taken into account.

Figure 10: The left panel shows the number of Auger electrons generated per incident electron by the Geant4-DNA ionisation process for the three physics constructors as a function of incident electron kinetic energy. The right panel shows the probability of K-shell ionisation of each constructor as a function of incident electron kinetic energy.

Table 1

	Geant4-DNA physics constructors electron models		
Process	**G4EmDNAPhysics_option2**	**G4EmDNAPhysics_option4**	**G4EmDNAPhysics_option6**
Ionisation (inelastic)	Emfietzoglou dielectric model (11 eV - 1 MeV) [5]	Emfietzoglou-Kyriakou dielectric model (10 eV - 10 keV) [47]	Relativistic Binary Encounter Bethe model from CPA100 code (11 eV - 256 keV) [48]
Electronic excitation (inelastic)	Emfietzoglou dielectric model (9 eV - 1 MeV) [5]	Emfietzoglou-Kyriakou dielectric model (8 eV - 10 keV) [47]	dielectric model from CPA100 code (11 eV - 256 keV) [48]
Elastic scattering (elastic)	partial wave model (7.4 eV - 1 MeV) [5]	Uehara screened Rutherford model (9 eV - 10 keV) [47]	Independent Atom Method model from CPA100 code (11 eV - 256 keV) [48]
Vibrational excitation (inelastic sub-excitation)	Sanche data (2 eV - 100 eV) [49]	n/a	n/a
Attachment (inelastic sub-excitation)	Melton data (4 eV - 13 eV) [50]	n/a	n/a
Auger electron emission	From the EADL database[51] and the Geant4 atomic relaxation interface [52,53]		
Default tracking cut(*)	7.4 eV	10 eV	11 eV

Table 1: Content of the three reference Geant4-DNA physics constructors for TS simulations of electrons in liquid water available in the Geant4 10.4 release. Processes and models are indicated as well as their energy range of applicability and main reference. Processes are identified as elastic, inelastic and inelastic sub-excitation processes. Auger emission is listed as a separate process. We also indicate the tracking cut below which the tracking of electrons is stopped and their remaining kinetic energy is locally deposited. (*): This tracking cut is handled by a specific Geant4-DNA process - so-called "G4DNAElectronSolvation" - which

does not apply when chemistry simulation is activated (electrons are tracked till thermalization and are considered as solvated).

Table 2

Extended example name	Purpose	Macro file	Other related reference(s)
dnaphysics	detail of tracking, automatic combination with Geant4 standard EM physics models, modification of medium density	dnaphysics.in	[6]
microdosimetry	combination “by hand” of Geant4 standard EM and Geant4-DNA processes and models in different regions	microdosimetry.in	[6]
range	range, projected range, penetration	range.in	[59]
spower	stopping power	spower.in	[72]
mfp	mean free path	mfp.in	-
wvalue	mean energy required for the creation of an ion pair in liquid water (the so-called "W-value")	wvalue.in	[47]
svalue	dose to a liquid water target per unit of cumulated activity in a source region (the so called "S-value")	svalue.in	[6,73,74]
slowing	slowing-down electron spectra	slowing.in	[72]
microyz	microdosimetric distributions (lineal energy y, specific energy z) and	microyz.in	[60]

	related quantities		
TestEm12(+)	dose point kernel	dna.mac	6,59,75
TestEm5(+)	identification of atomic de-excitation products for Geant4-DNA processes	dna.mac	-

Table 2: List of Geant4-DNA "extended" examples available for TS simulations in liquid water. These examples are available in Geant4 release 10.4 (December 2017). The Geant4-DNA macro files used to obtain most of the results presented in this work are given. Other related references are indicated as well. (+): These examples are not specific to Geant4-DNA but are equipped with Geant4-DNA macro files for TS simulations.

Table 3

Physical process	Geant4-DNA electron model	Geant4 electron standard electromagnetic model
Elastic	partial wave (< 1 MeV)	Urban (multiple scat., > 1 MeV) or Coulomb (single scat., > 1 MeV)
Electronic excitation	Emfietzoglou-Kyriakou (< 10 keV) and default (10 keV - 1 MeV)	n/a
Ionisation	Emfietzoglou-Kyriakou (< 10 keV) and default (10 keV - 1 MeV)	Moller-Bhabha (> 1 MeV)
Vibrational excitation	Sanche (< 100 eV)	n/a
Attachment	Melton (< 13 eV)	n/a

Table 3: Description of the automatic combination of Geant4-DNA models with Geant4 standard electromagnetic models for electrons in liquid water, performed by the "G4EmDNAPhysicsActivator" interface available from Geant4 10.4 release (December 2017), and illustrated in the "dnaphysics" example.

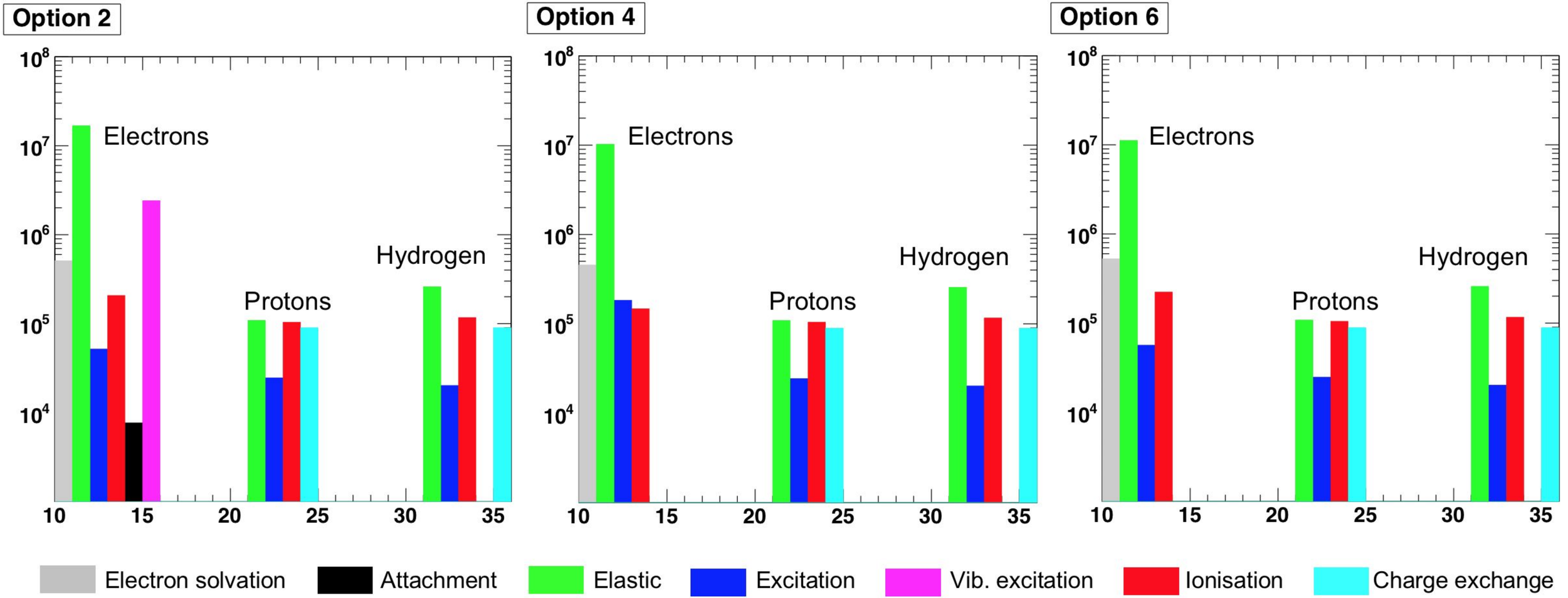
Option 2
Option 4
Option 6
Electrons
Protons
Hydrogen
10^8
10^7
10^6
10^5
10^4
10
15
20
25
30
35
Electron solvation
Attachment
Elastic
Excitation
Vib. excitation
Ionisation
Charge exchange

Distance (nm)

10^7
10^6
10^5
10^4
10^3
10^2
10
1

electron - ICRU90
proton - ICRU90
alpha - ICRU90

Option 2
Option 4
Option 6

10
10^2
10^3
10^4
10^5
10^6

E (eV)

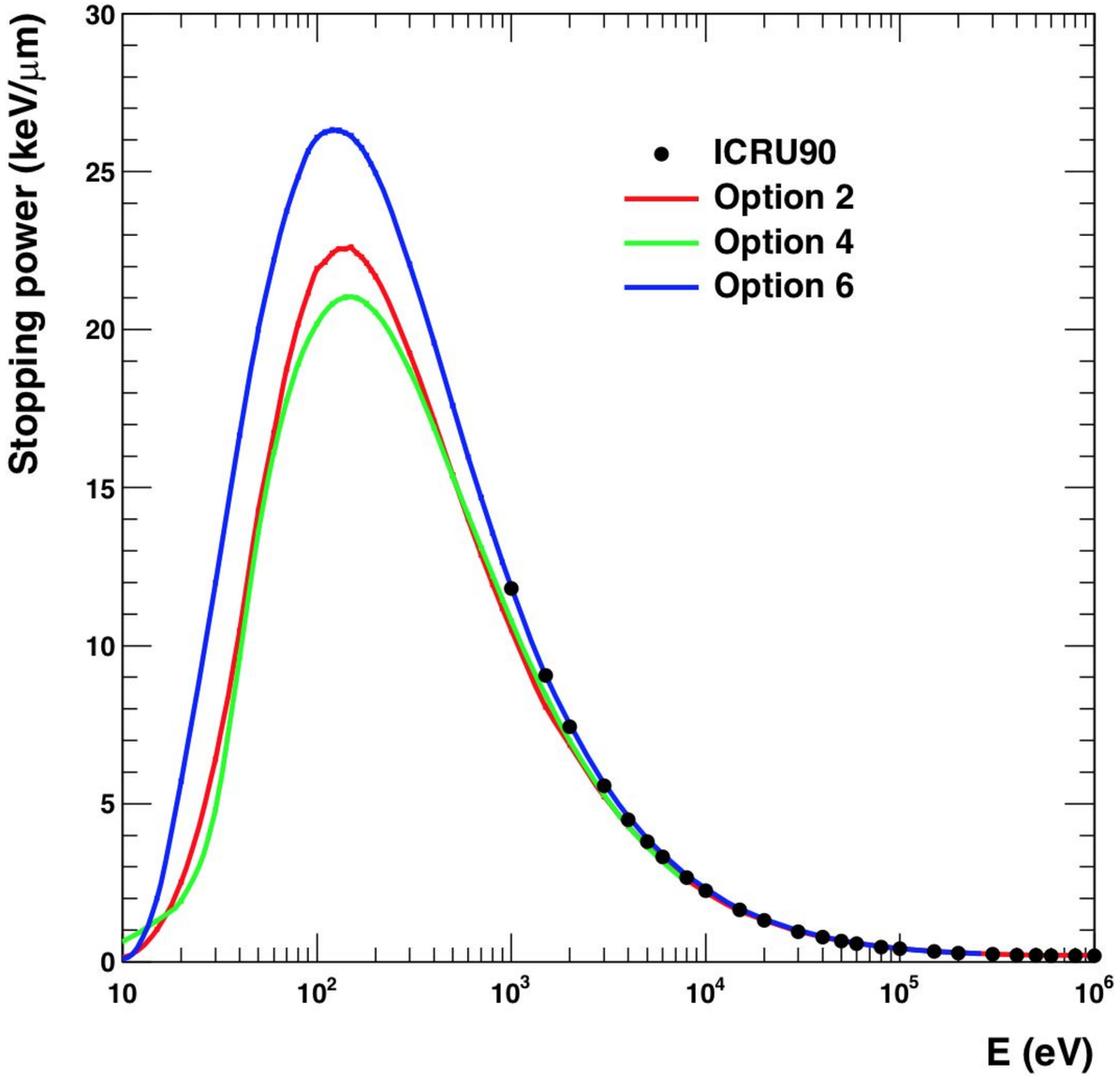
Stopping power (keV/μm)
E (eV)
ICRU90
Option 2
Option 4
Option 6

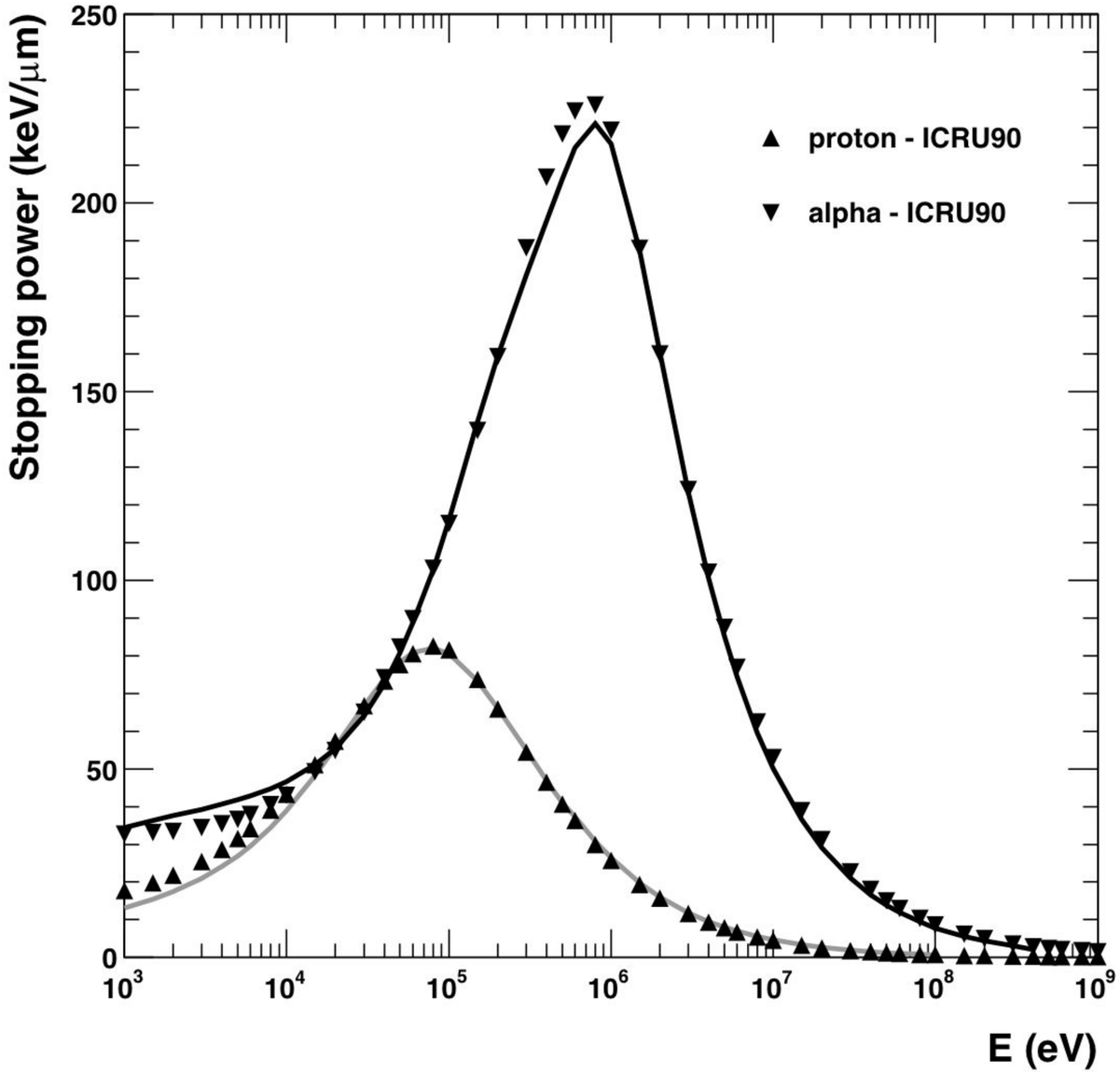
Stopping power (keV/μm)
E (eV)
proton - ICRU90
alpha - ICRU90

Mean free path (nm)

10^3

10^2

10

1

10^{-1}

Option 2

Option 4

Option 6

10

10^2

10^3

10^4

10^5

10^6

E (eV)

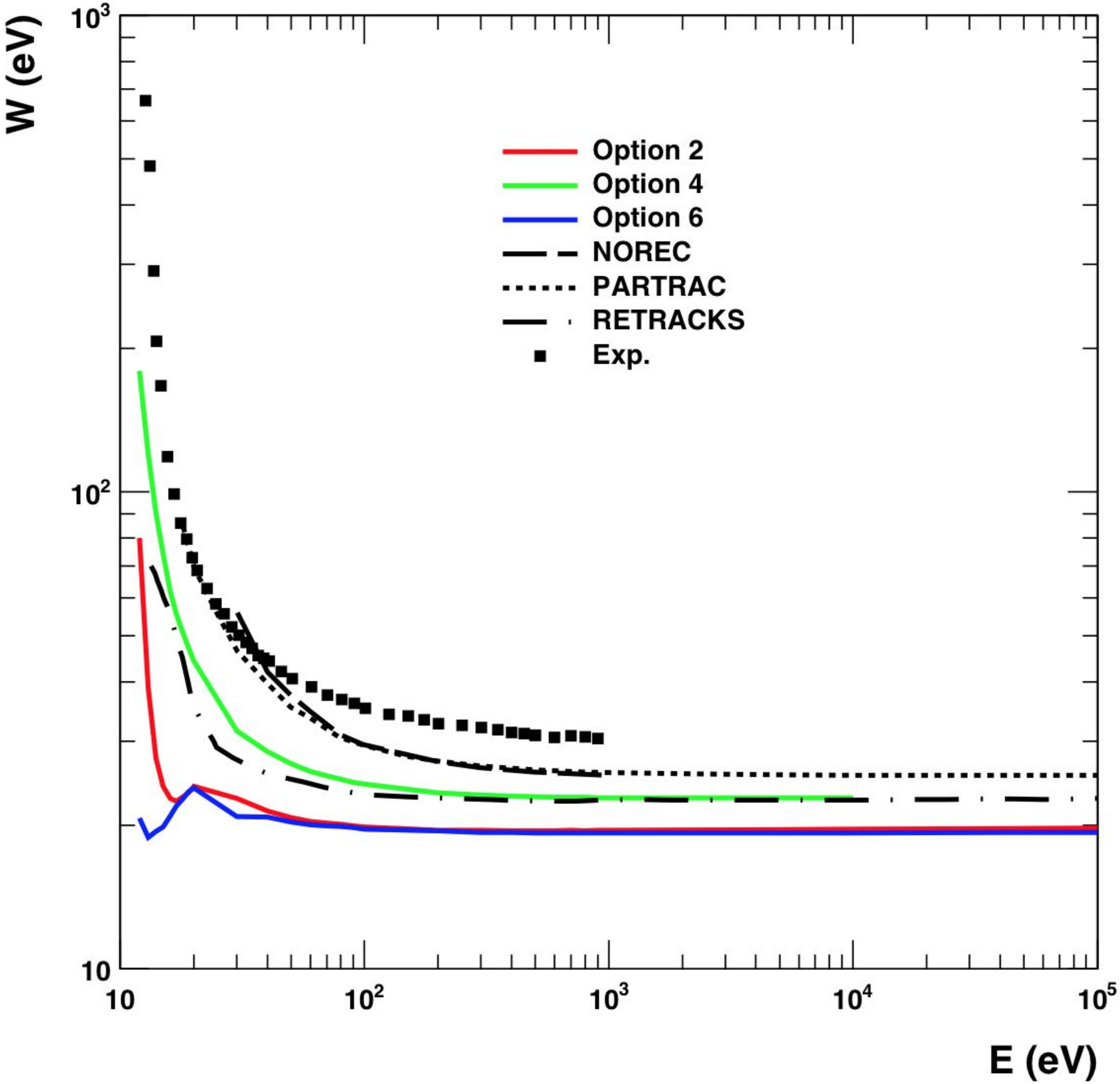
W (eV)
10^3
10^2
10
10
10^2
10^3
10^4
10^5
E (eV)
Option 2
Option 4
Option 6
NOREC
PARTRAC
RETRACKS
Exp.

S (Gy/Bq.s)

10^{-2}

10^{-3}

10^{-4}

10^{-5}

10^{-6}

10^{-7}

10^{-8}

N ← N

N ← Cy

Option 2

Option 4

Option 6

★ MIRD

Cy

N

10^{2}

10^{3}

10^{4}

E (eV)

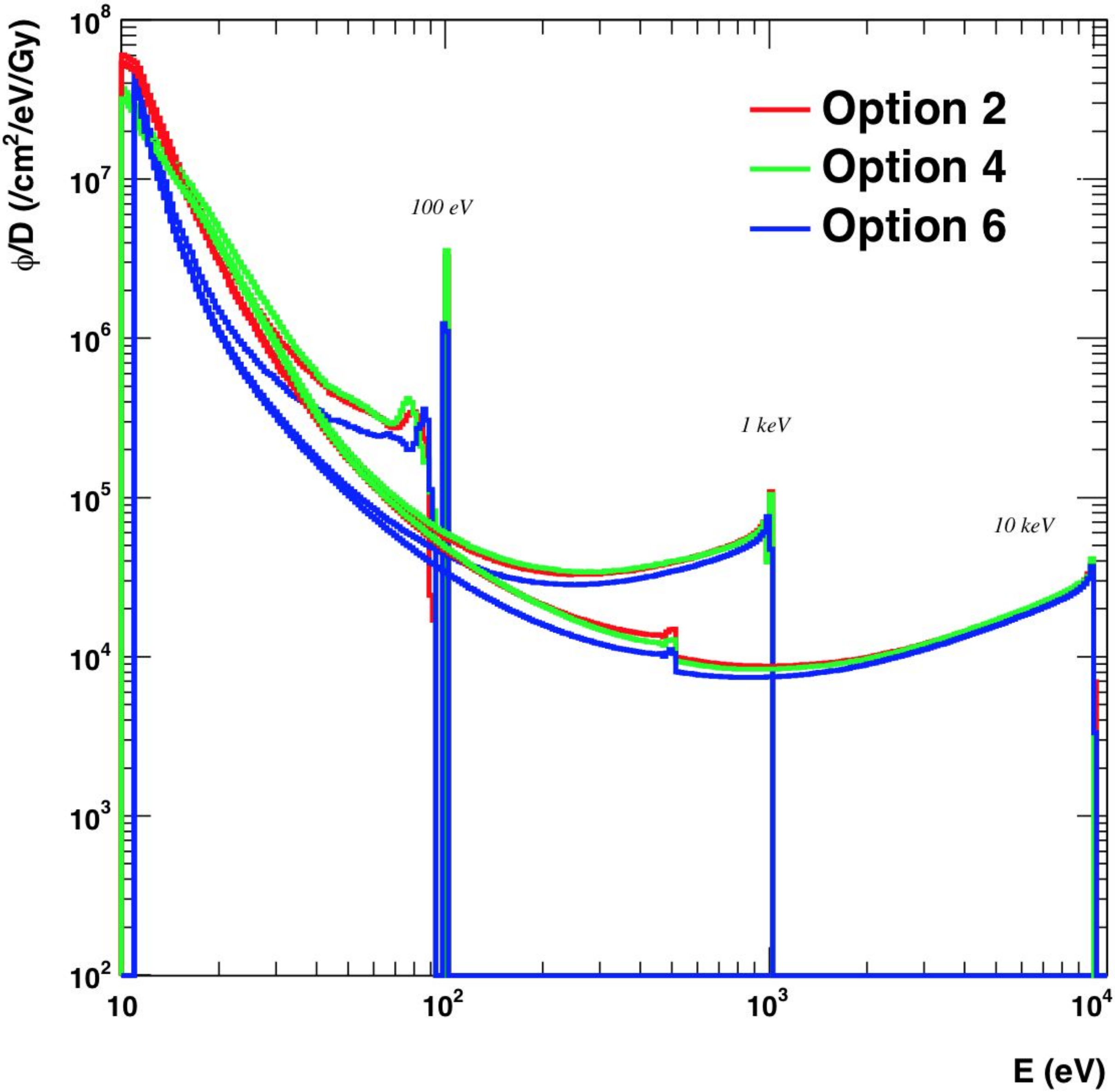
ϕ/D (/cm²/eV/Gy)
10⁸
10⁷
10⁶
10⁵
10⁴
10³
10²
10
10²
10³
10⁴
E (eV)
Option 2
Option 4
Option 6
100 eV
1 keV
10 keV

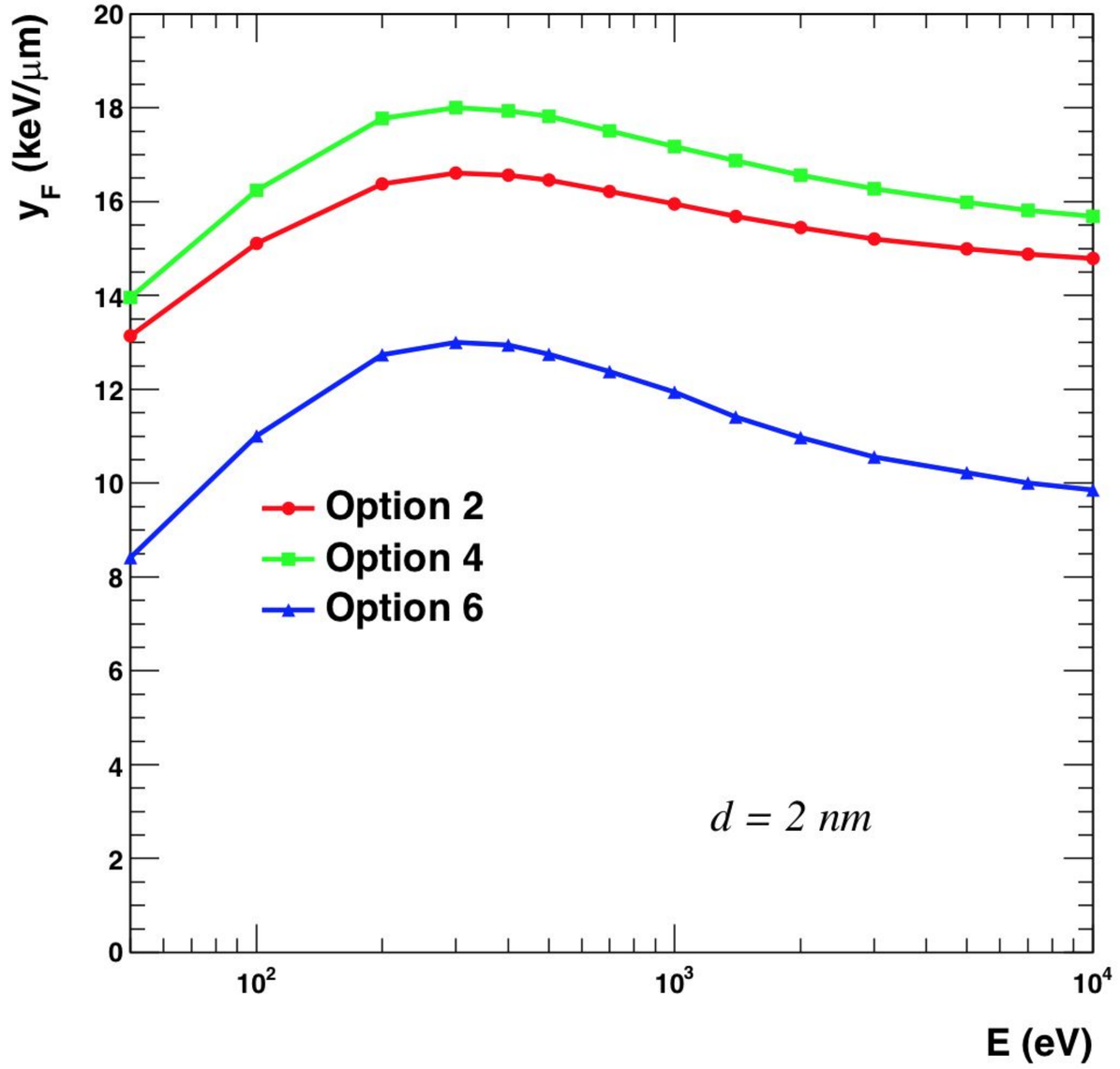
y_F (keV/μm)
E (eV)
Option 2
Option 4
Option 6
d = 2 nm

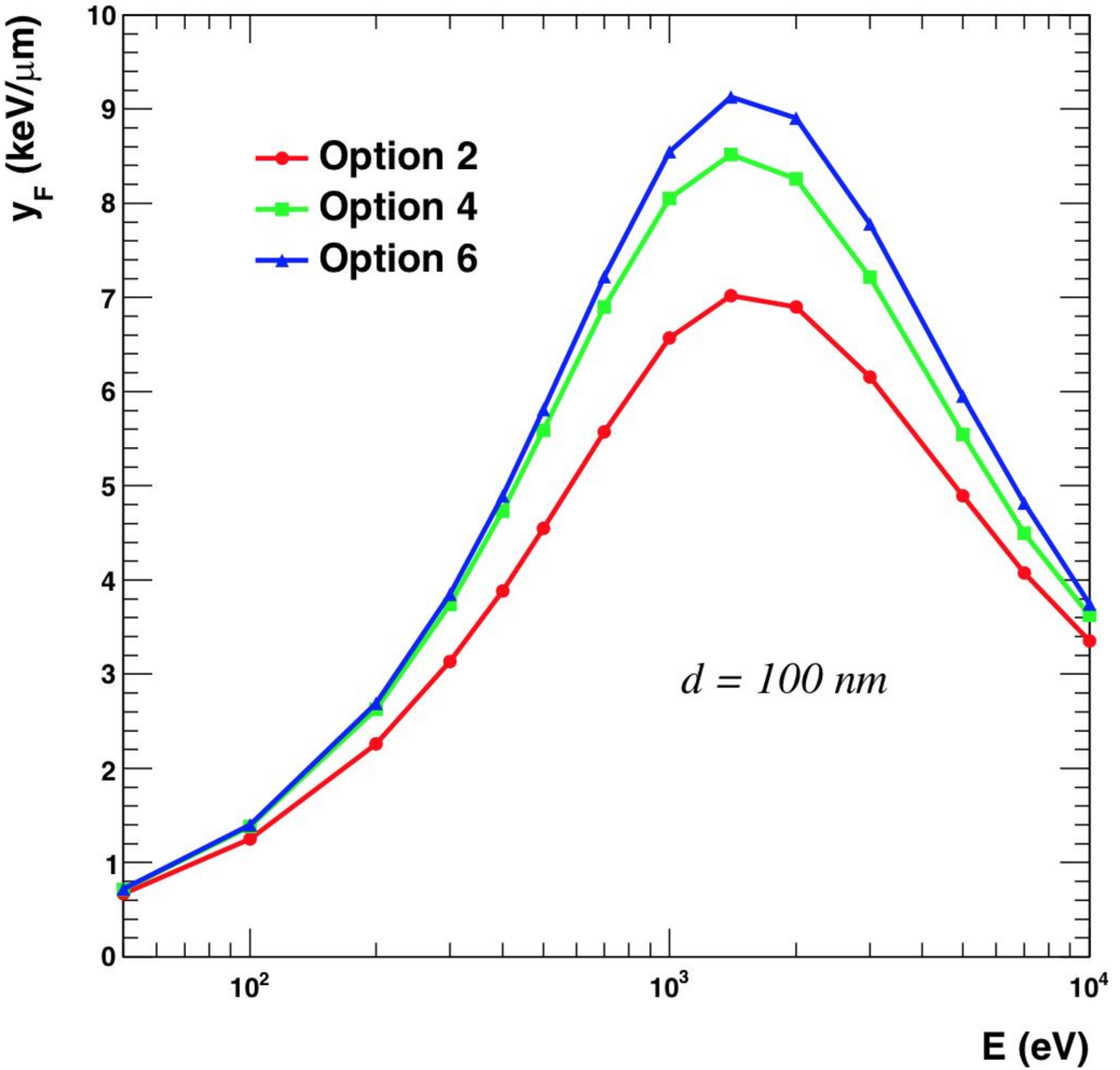
y_F (keV/μm)
E (eV)
Option 2
Option 4
Option 6
d = 100 nm

DPK (keV/μm)

10^2

10

1

10^{-1}

10^{-2}

10^{-3}

1 keV

100 eV

Option 2

Option 4

Option 6

0 10 20 30 40 50 60 70 80 90 100

r (nm)

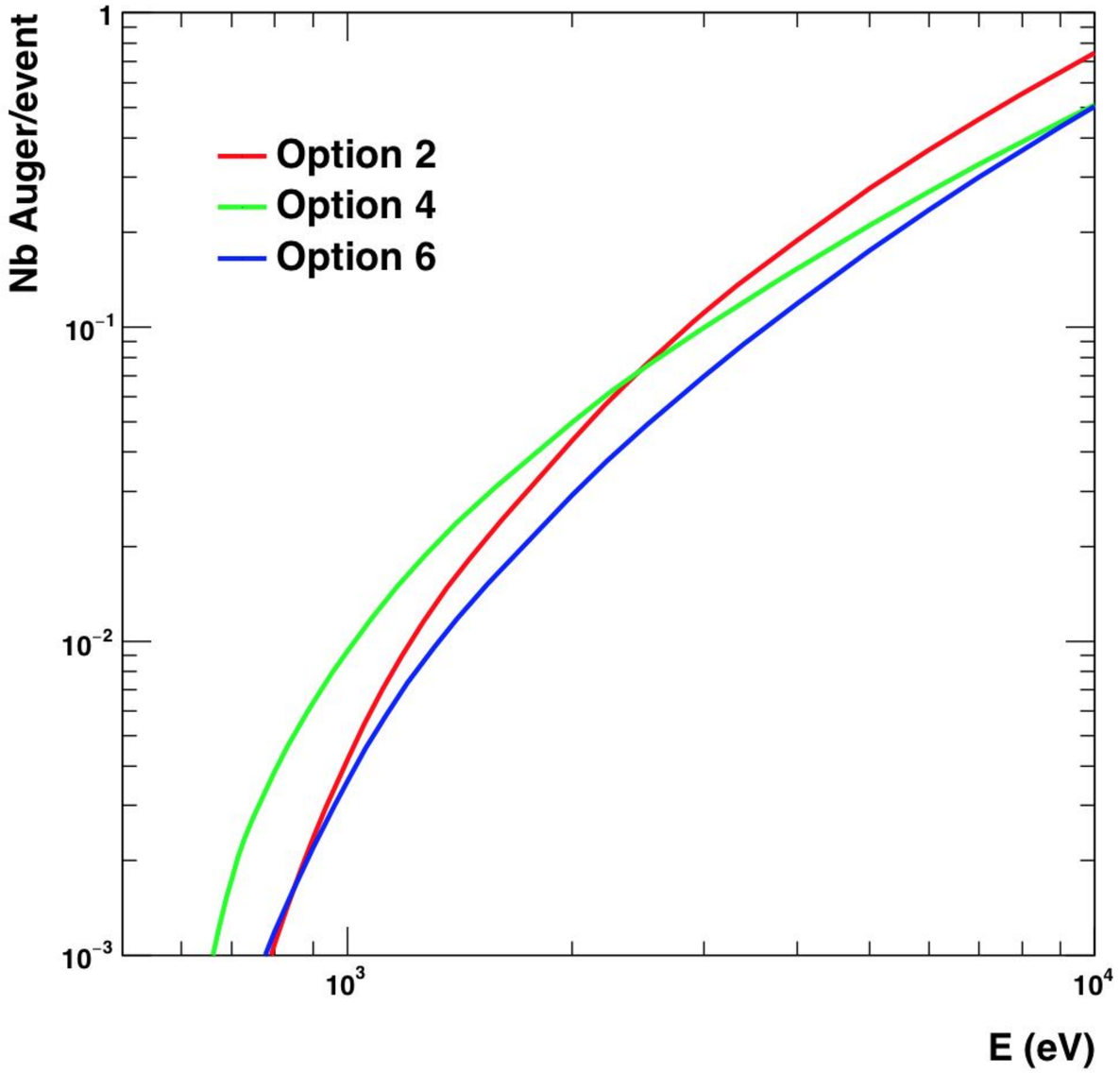
Nb Auger/event
1
10^{-1}
10^{-2}
10^{-3}
Option 2
Option 4
Option 6
10^{3}
10^{4}
E (eV)

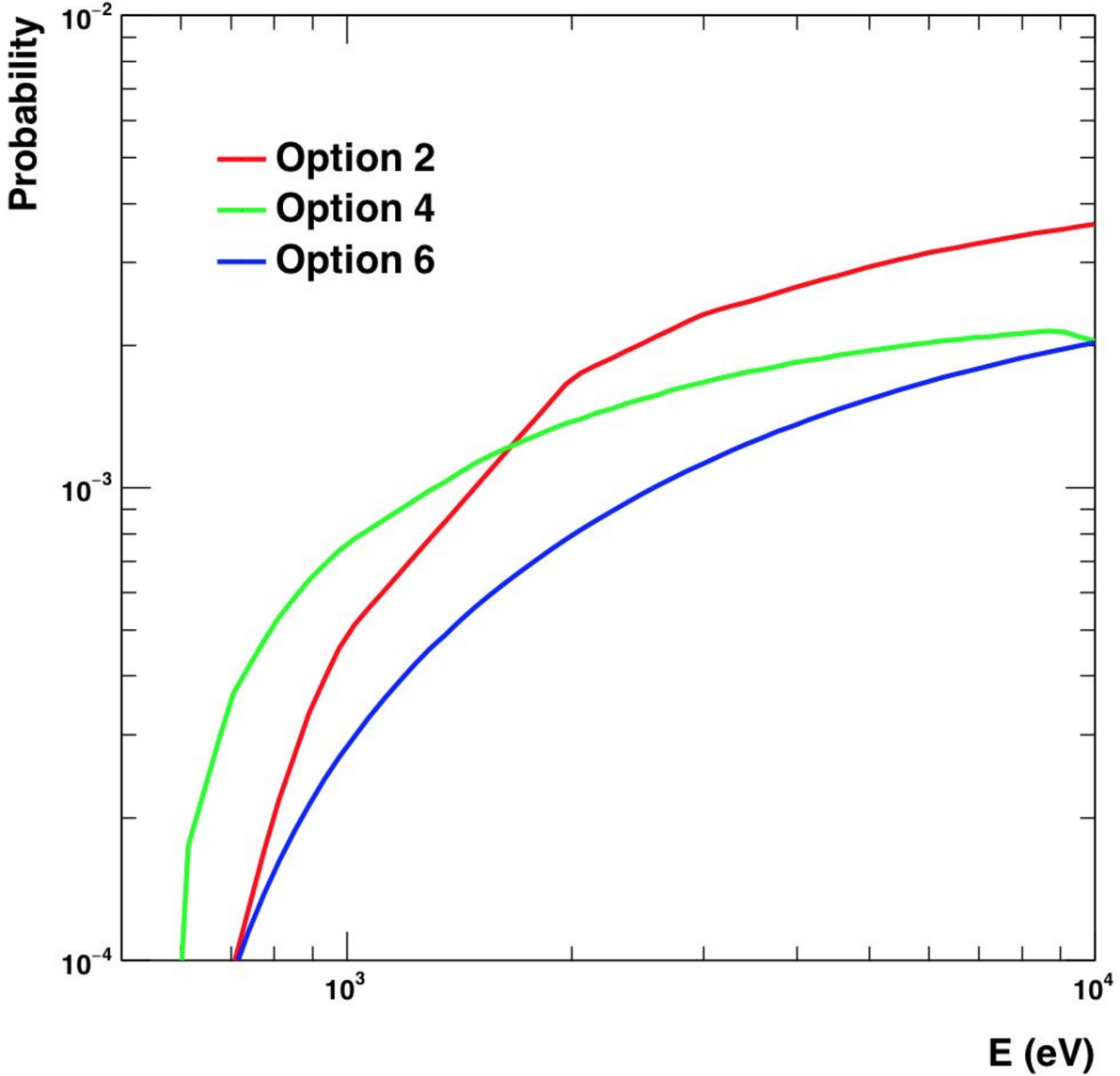
Probability
10^{-2}
10^{-3}
10^{-4}
Option 2
Option 4
Option 6
10^{3}
10^{4}
E (eV)

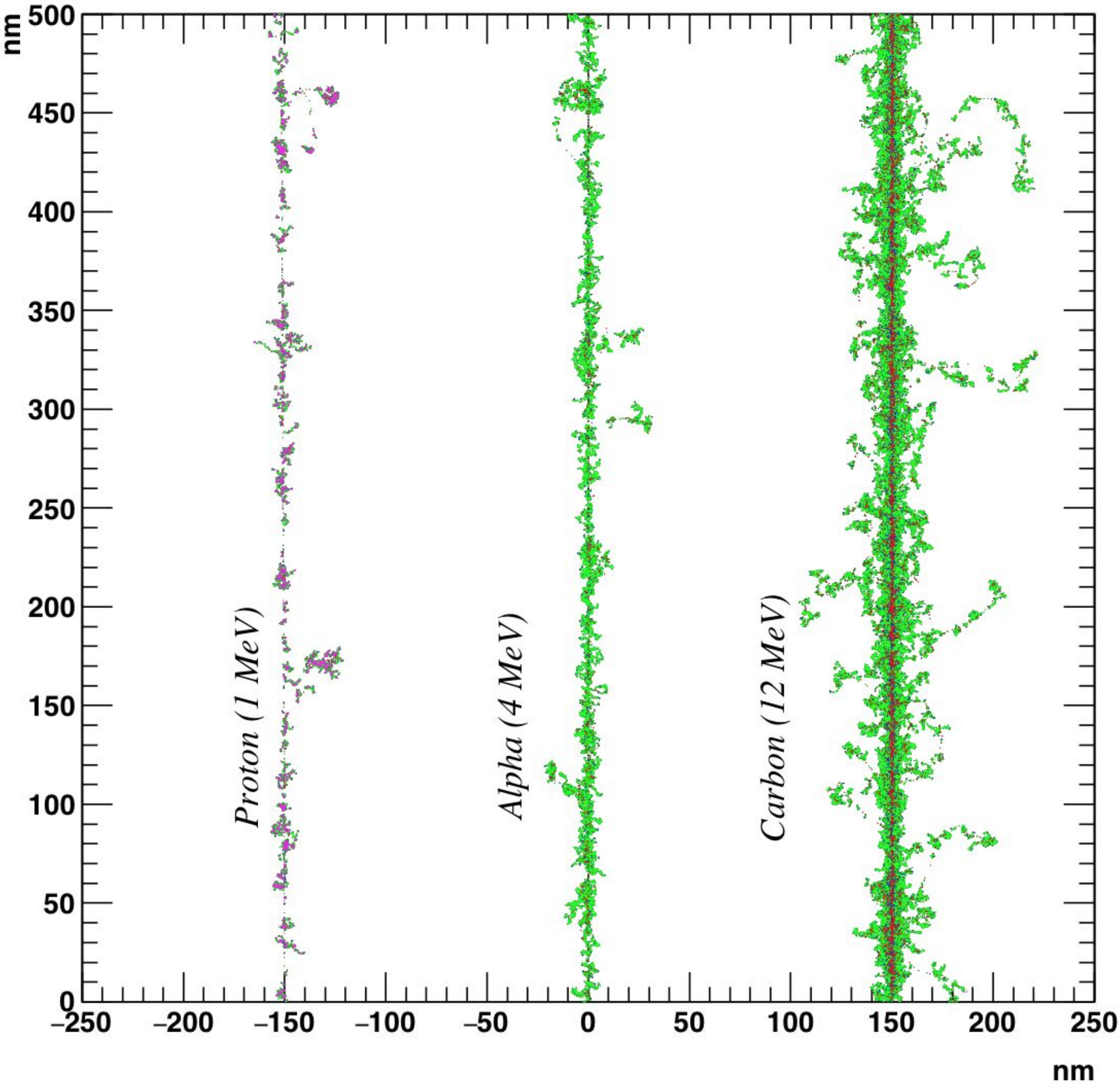
nm
500
450
400
350
300
250
200
150
100
50
0
−250
−200
−150
−100
−50
0
50
100
150
200
250
nm
Proton (1 MeV)
Alpha (4 MeV)
Carbon (12 MeV)